THE ASTROPHYSICAL JOURNAL, 415:652–671, 1993 October 1

FORBIDDEN VELOCITY GAS DETECTED IN ULTRAVIOLET INTERSTELLAR ABSORPTION TOWARD FOUR DISTANT INNER GALAXY STARS

TODD M. TRIPP,[1] KENNETH R. SEMBACH,[1,2,3] AND BLAIR D. SAVAGE[1,2]
Received 1992 December 28; accepted 1993 April 2

ABSTRACT

We analyze *International Ultraviolet Explorer* high-dispersion observations of interstellar absorption toward HD 167402, HD 168941, HD 172140, and HD 173502, four distant, inner Galaxy, lower halo/thick disk stars ($2\overset{\circ}{.}3 < l < 5\overset{\circ}{.}8$, $6\overset{\circ}{.}3 < |b| < 12\overset{\circ}{.}3$). On the basis of ultraviolet stellar photospheric and wind lines, we classify HD 167402, HD 168941, HD 172140, and HD 173502 as B0 II/B0.5 Ib, O9.5–9.7 II–III, B0.5 III, and B0.5 III, respectively. These classifications result in line-of-sight distance estimates ranging from 6.1 to 6.8 kpc $\pm 25\%$, and therefore the stars are 0.69 to 1.5 kpc below the Galactic plane. Low and high ion interstellar absorption profiles (including high resolution and high S/N optical Ca II profiles) observed toward three of the four stars show significant amounts of absorption at negative velocities. Negative velocities are not allowed by normal Galactic rotation in the directions sampled. If the thick disk/lower halo gas is corotating with the thin disk and has a radial velocity dispersion of ~ 30 km s^{-1}, then we would expect the absorption profiles observed with the *IUE* to extend from -40 to $+100$ km s^{-1} in these directions. However, the observed profiles extend from roughly -100 to $+100$ km s^{-1}. We discuss some viable interpretations of the negative (i.e., forbidden) velocity gas. The most plausible interpretation is that the absorption at negative velocities occurs in outflowing gas, a few hundred parsecs from the plane, associated with the 3 kpc arm. This negative velocity gas is consistent with the recent numerical studies by Martos and Cox of gas flows in the vicinity of spiral arms. The HD 167402 and HD 168941 observations, based on multiple *IUE* spectra, reveal strong absorption by N V, C IV, and Si IV. The clear presence of N V absorption implies the existence of hot ($T \sim 2 \times 10^5$ K) collisionally ionized gas along these inner Galaxy sight lines. The strong Si IV absorption appears to require an additional source of photoionization. The self-ionizing radiation produced by hot cooling gas is a likely possibility.

Subject headings: Galaxy: kinematics and dynamics — ISM: abundances — ultraviolet: interstellar

1. INTRODUCTION

This is the fourth in a series of papers presenting detailed analyses of *International Ultraviolet Explorer* (*IUE*) high-dispersion observations of interstellar absorption toward distant Milky Way halo stars. Previous papers in this series have studied interstellar absorption toward HD 163522 (Savage, Massa, & Sembach 1990; hereafter Paper I), HD 156359 (Sembach, Savage, & Massa 1991; hereafter Paper II), and 12 sight lines in the Galactic halo (Sembach & Savage 1992; hereafter Paper III). The goals of this program are to learn about the origin, ionization, and kinematics of highly ionized gas in the Galactic disk and halo, and to contribute to ongoing efforts to determine the distribution of interstellar species accessible only to ultraviolet instruments. The large column densities accumulated on the long paths enhance our ability to detect high ion absorption with the *IUE*, and by combining multiple exposures offset along the long axis of the large aperture, we reduce fixed pattern noise in the composite spectra and achieve signal-to-noise ratios of ≈ 15 to 25.

In this paper we concentrate on the kinematics of interstellar gas at moderate distances from the plane. Understanding the kinematics of the Galactic halo gas is an important step toward understanding broader issues such as the origin and support of the halo or the relationship between absorption in "normal" (i.e., Milky Way-type) gaseous halos and the halos probed by QSO absorption lines. The overall motion of interstellar gas over long path lengths is predominantly due to the rotation of the Galaxy, but additional mechanisms which may significantly affect the gas kinematics include Galactic fountains and chimneys, Galactic structure (e.g., flows associated with spiral arms or a bar in the Galactic center), and large-scale gas flows such as a Galactic wind.

We have used the *IUE* satellite to search for evidence of radial inflow or outflow from the inner Galaxy, and in this paper we present our findings. We have concentrated on four lower halo stars near the Galactic center, HD 167402 ($l = 2\overset{\circ}{.}3$, $b = -6\overset{\circ}{.}4$), HD 168941 ($l = 5\overset{\circ}{.}8$, $b = -6\overset{\circ}{.}3$), HD 172140 ($l = 5\overset{\circ}{.}3$, $b = -10\overset{\circ}{.}6$), and HD 173502 ($l = 5\overset{\circ}{.}4$, $b = -12\overset{\circ}{.}3$), in order to minimize the effects of Galactic rotation and more easily isolate evidence of inflow or outflow from other effects such as decoupling of halo corotation or stellar distance uncertainties. In § 2 we present the observations and data reduction. In § 3 we discuss the stellar spectra; we review the stellar classifications and examine the degree of contamination of the interstellar absorption features by stellar absorption lines. In § 4 we analyze the interstellar spectra using the apparent optical depth technique. We evaluate the equivalent widths and column densities of the high ion absorption lines, and we discuss the velocity structure in the profiles of the low- and high-ionization stages placing particular emphasis on the significant amount of gas detected at forbidden velocities. We

[1] Washburn Observatory, Department of Astronomy, University of Wisconsin–Madison, 475 North Charter Street, Madison, WI 53706-1582.
[2] Guest Observer with the *International Ultraviolet Explorer* Satellite, sponsored and operated by the National Aeronautics and Space Administration (USA), the Science and Engineering Research Council (UK), and the European Space Agency.
[3] Currently a Hubble Fellow at the Center for Space Research, Massachusetts Institute of Technology, Building 37, Cambridge, MA 02139.

TABLE 1

HIGH-DISPERSION *IUE* SPECTRA

Object	Image Number	Observation Date (Day, Year)	Exposure Time (minutes)	Position of Star in Aperture[a]	Velocity Shift[b] (km s^{-1})
HD 167402.....	SWP 23528	210,1984	160	Center	0
	SWP 42270	229,1991	160	+5″ offset	−31
	SWP 42271	229,1991	140	−5″ offset?	0
	SWP 42277	230,1991	120	Center	0
	SWP 42288	231,1991	140	−5″ offset	+8
HD 168941.....	SWP 23843	245,1984	270	Center	0
	SWP 41374	103,1991	245	−5″ offset	+17
	SWP 42263	228,1991	220	Center?	−17
	SWP 42264	228,1991	165	−5″ offset	+7
	SWP 42287	231,1991	200	+5″ offset	−35
HD 172140.....	SWP 22506	77,1984	210	Center	0
HD 173502.....	SWP 09816	229,1980	116	Center?	−30
	SWP 23866	247,1984	190	Center	0

[a] Spectra were offset by ±5″ along the long axis of the 10″ × 20″ aperture in order to reduce fixed pattern noise in the combined spectrum.

[b] The velocity shift applied to each spectrum to bring them into a common heliocentric velocity system (i.e., $v_{helio} = v_{obs}$ + velocity shift).

discuss the sight line properties in § 5, the kinematics in § 6, and the physical conditions and ionization of the interstellar gas in § 7. We summarize the results in § 8.

2. OBSERVATIONS AND DATA REDUCTION

A summary of the *IUE* high-dispersion data used for this study is given in Table 1. The stars observed have been studied previously by Savage & Massa (1987) and Danly et al. (1992). We have retrieved the spectra used by those authors from the *IUE* data archives, and we have obtained new observations of HD 167402 and HD 168941 in order to improve the signal-to-noise. Following the procedure employed in Papers I–III, we have acquired new individual exposures with the star offset along the long axis of the large (10″ × 20″) aperture. By co-adding these spectra after correcting for the offset, the *IUE* fixed pattern noise (see Harris & Sonneborn 1987, and references therein) is reduced and the signal-to-noise is improved from ∼5–10 (typical single exposure S/N) to ∼15–25 (see Fig. 3 in Paper III).

The data reduction procedure is described in detail in Papers II and III and is briefly summarized here. We first put the various observations of a given star into a common velocity reference frame by aligning five to nine strong interstellar absorption lines. This accounts for intentional object offsets in the large aperture. A single velocity shift is applied to each spectrum, and we use the most recent aperture-centered observation as the template (i.e., unshifted) spectrum, except for the case of HD 168941. For HD 168941, we used SWP 23843 as the template since the cores of the low ionization lines of S II and Si II derived from the SWP 42263 spectrum are clearly offset from the cores of the H I 21 cm emission profile observed by Danly et al. (1992) and the Na I and Ca II absorption profiles observed by Sembach, Danks, & Savage (1993) toward this star. The S II and Si II profiles derived from the SWP 23843 spectrum show no such offset. We also checked the S II and Si II profiles for the template spectra of HD 167402 and HD 173502 against the optical and radio profiles and find that they show no substantial offsets. We therefore believe that our velocity scale is accurate to approximately ±5 km s^{-1}. The excessive background subtraction below 1400 Å due to interorder scattered light is accounted for according to the scheme outlined by Bianchi & Bohlin (1984), and the multi-order ripple correction given by Barker (1984) is also applied. Data spikes (cosmic rays and hot pixels) are automatically filtered out (see Paper III). The spectra are co-added in *IUE* intensity units in order to weight each spectrum by its exposure duration. A second velocity shift, Δv_{LSR}, is applied to the composite spectrum to bring it into the reference frame of the local standard of rest (LSR). The values of Δv_{LSR} ($= v_{LSR} - v_{Helio}$) were calculated assuming the Sun is moving toward $l = 53°$, $b = 25°$ at a speed of +16.5 km s^{-1} (Mihalas & Binney 1981) and are given in Table 2. The radiation-induced background was high during the exposure of SWP 42264, but we elected to include this

TABLE 2

STELLAR AND INTERSTELLAR DATA

Object HD	l	b	MK	V	$E(B-V)$	d (kpc)	z (kpc)	$v_r(d)$ (km s^{-1})	$v_r(*)$ (km s^{-1})	$v \sin i$ (km s^{-1})	Δv_{LSR} (km s^{-1})	log N_α (cm^{-2})	$\langle n_{H\,I} \rangle$ (cm^{-3})
167402.....	2.3	−6.4	B0 II/B0.5 Ib	8.95	0.25	6.6	−0.80	+27	+45	<50	8.6	20.99	0.05
168941.....	5.8	−6.3	O9.5–9.7 II–III	9.34	0.37	6.1	−0.69	+45	+114	140	9.3	21.11	0.07
172140.....	5.3	−10.6	B0.5 III	9.96	0.22	6.8	−1.3	+62	+60	150	8.6	21.11	0.06
173502.....	5.4	−12.3	B0.5 III	9.68	0.17	6.3	−1.5	+43	+76	50	8.4	20.98	0.05

NOTES.—N_α is the total interstellar neutral hydrogen column density determined from H I Lyman-α absorption (from Diplas & Savage 1993), and $\langle n_{H\,I} \rangle$ is the average number density of neutral hydrogen.

exposure in the composite spectrum after inspection of the SWP 42264 spectrum. Excluding SWP 42264 from the composite has a negligible effect.

The relative intensities of interstellar absorption lines observed in the HD 167402, HD 168941, HD 172140, and HD 173502 spectra are shown in Figures 1–4, respectively. High resolution ground-based observations of the Na I and Ca II interstellar absorption profiles observed by Sembach et al. (1993) toward these stars are shown in Figures 5 and 6. Galactic coordinates, line-of-sight distance (d), distance of the star from the plane (z), and stellar information {MK spectral type, projected rotational velocity ($v \sin i$), stellar radial velocity with respect to the LSR [v_R(*)], visual magnitude, and color excess} for these stars are tabulated in Table 2. We also list in Table 2 some properties of the interstellar medium {neutral hydrogen column density measured by Diplas & Savage 1993 from H I Lyman-α absorption (N_a) and the expected radial velocity, with respect to the LSR, of corotating gas at the distance of the star [$v_R(d)$]} for each sight line. Notice that HD 167402, HD 172140, and HD 173502 have stellar radial velocities that are comparable to the velocities predicted for corotating gas at the distances of the stars, which suggests that the derived distances are reasonable. HD 168941, however, has a higher stellar radial velocity and may be a runaway star. However, if HD 168941 is ~15% farther away than the distance listed in Table 2, then this high radial velocity would be expected (see Fig. 12). The

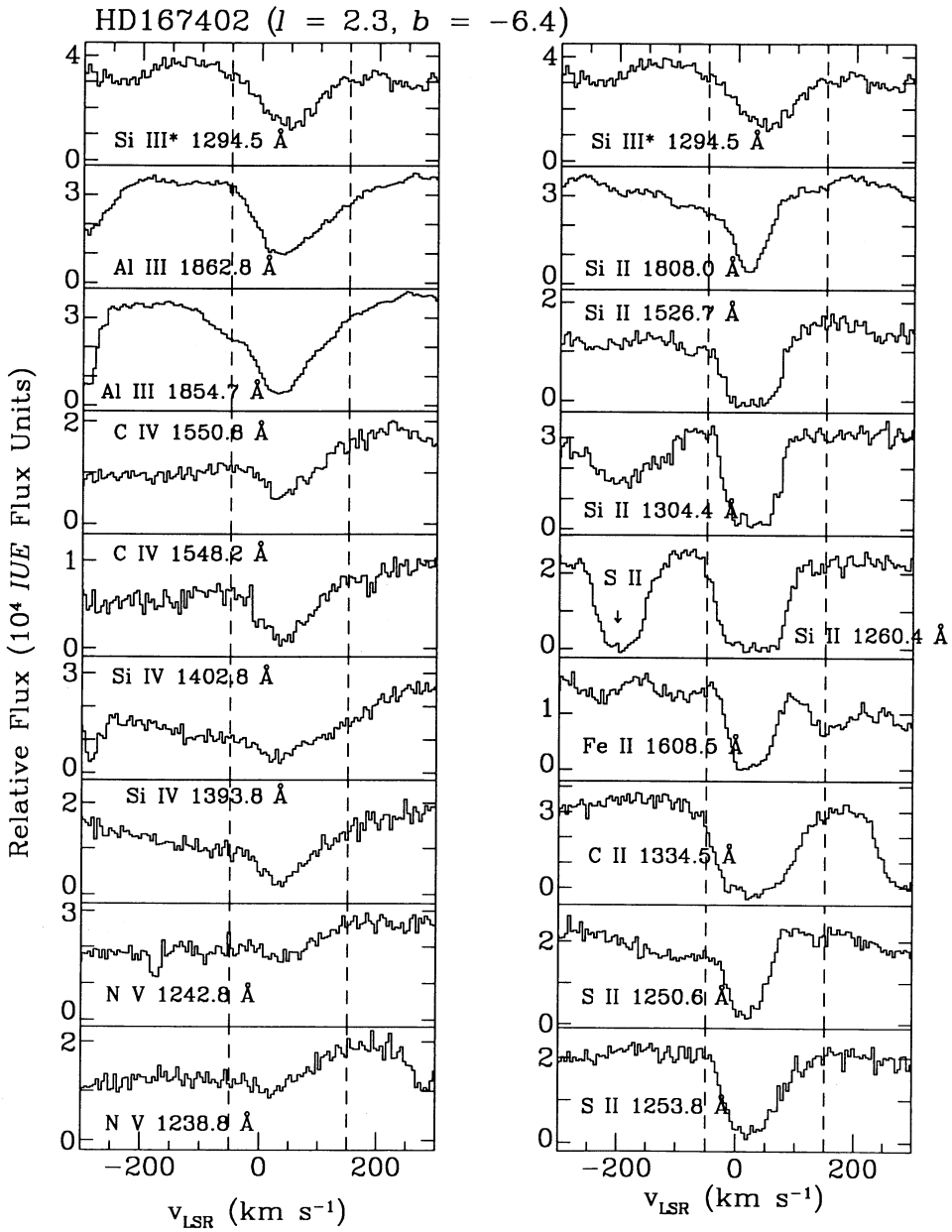

FIG. 1.—Selected interstellar absorption lines observed toward HD 167402 (relative flux vs. LSR velocity). The five observations listed in Table 1 have been combined to produce the profiles shown in this figure. The purely photospheric Si III* 1294.5 Å stellar absorption line is shown in the top panels so that the reader may visually compare the positions and profile shapes of the interstellar and stellar lines. The dashed vertical lines indicate the velocity extent of the C IV absorption profiles for comparison with the velocity extent of the other interstellar profiles.

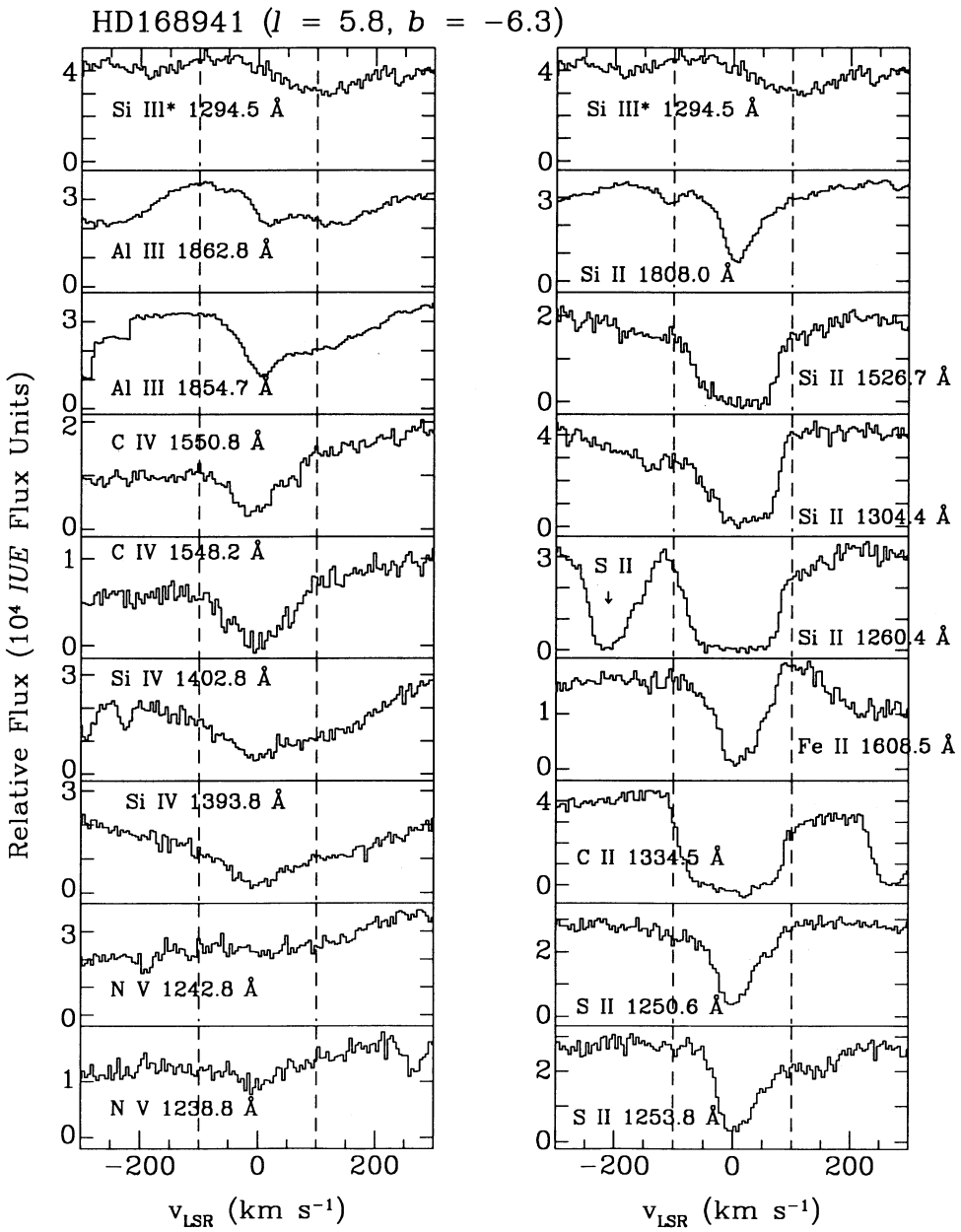

FIG. 2.—Selected interstellar absorption lines observed toward HD 168941. The five observations listed in Table 1 have been combined to produce the profiles shown in this figure. As in Fig. 1, the dashed vertical lines indicate the velocity extent of the C IV absorption, and the stellar Si III* 1294.5 Å line is illustrated in the top panels for comparison with the interstellar lines. Notice the significant amount of absorption at negative (i.e., forbidden) velocities.

wavelengths and oscillator strengths of the interstellar transitions shown in Figures 1–4 can be found in Morton (1991).

3. STELLAR SPECTRA

3.1. *Stellar Classification and Distance Estimations*

It is important to have reliable stellar classifications because we use these to estimate the distance to each star. The ultraviolet spectrum of a star can be used to evaluate the reliability of the MK temperature and luminosity classification assigned on the basis of optical data. A variety of temperature and luminosity diagnostics are present in the C, N, Al, Si, and Fe lines found between 1200 and 2000 Å. Examples of how the diagnostic information in the UV photospheric and wind lines can be extracted are found in the previous papers in this series and the references contained therein. We discuss several of these diagnostics briefly as part of our assessment of the spectral classification for HD 167402, HD 168941, HD 172140, and HD 173502.

3.1.1. *HD 167402*

The Si III 1300 Å multiplet is one of the best temperature diagnostics available in the spectra of early B stars (Massa 1989). Its strength in the spectrum of HD 167402 implies that the star has a spectral type between B0 and B1. The Si II 1264 Å line is also sensitive to temperature and becomes prominent in

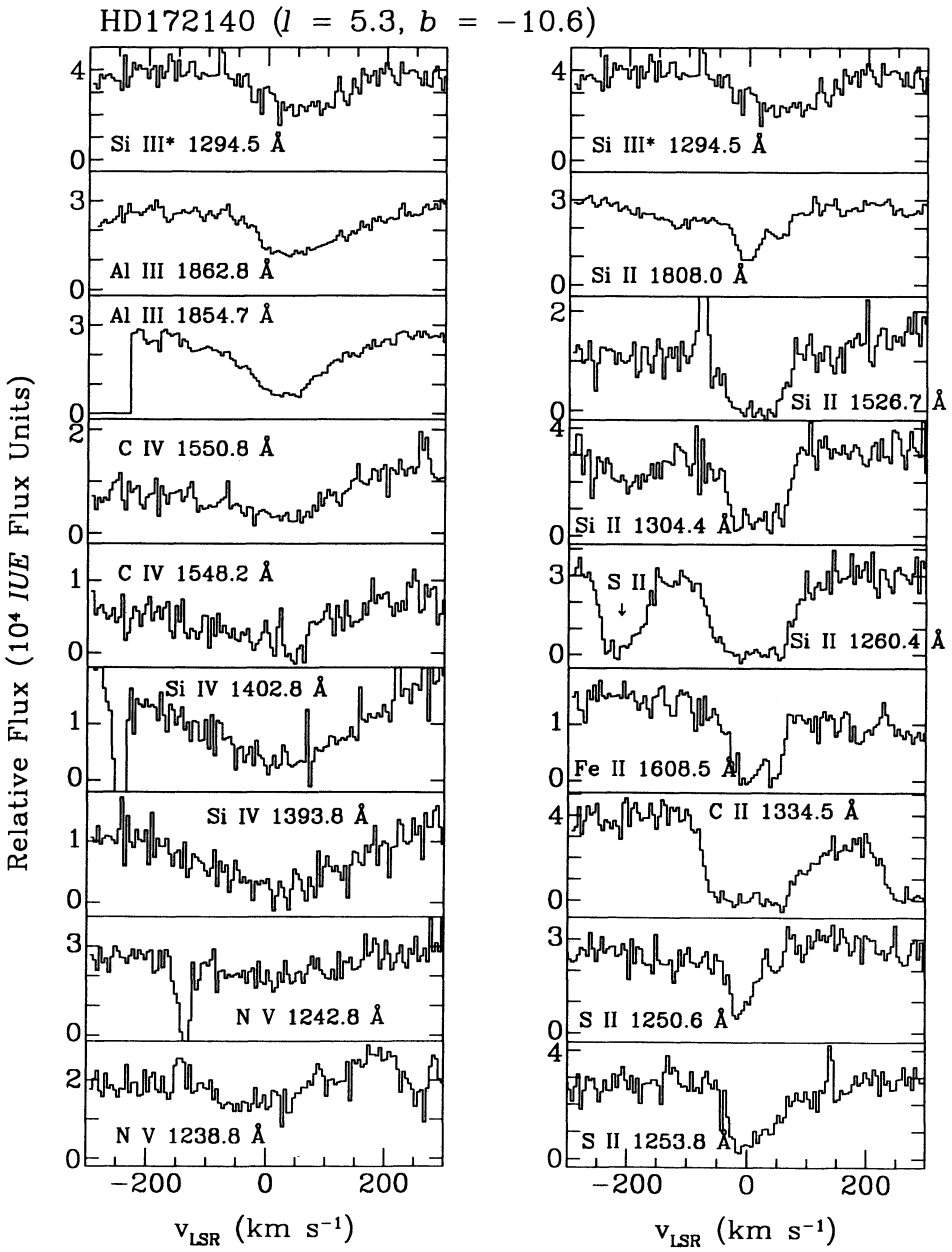

FIG. 3.—Selected interstellar absorption lines observed toward HD 172140, as in Fig. 1

the spectra of stars with spectral types later than B1 (Massa 1989). It is very weak in the HD 167402 spectrum, again indicating that the star has a spectral type earlier than B1. The strength of the N IV 1718 Å line is also indicative of an early B star. The Si III 1417 Å line shows a strong positive luminosity effect at these spectral types (Massa 1989) and is strong in the HD 167402 spectrum, which suggests that the star is more luminous than a class III star.

The C IV (1548, 1550 Å), N V (1238, 1242 Å), and Si IV (1393, 1402 Å) wind lines in the spectrum of HD 167402 also place constraints on its luminosity classification. The wind lines are known to be sensitive luminosity indicators in late O and early B stars (Walborn & Panek 1984; Walborn, Nichols-Bohlin, & Panek 1985; Heck 1987). The combination of a well-developed C IV profile and a Si IV profile that is just beginning to develop is representative of a class II star at a spectral type of B0 or a class Ib star at a spectral type of B0.5. The N V wind profile also suggests a luminosity classification of Ib or II.

Garrison, Hiltner, & Schild (1977) classified HD 167402 as a B0 Ib star. From the ultraviolet spectrum, we assign a classification of B0 II/B0.5 Ib.

3.1.2. *HD 168941*

The Si III 1300 Å lines seen in the spectrum of HD 168941 are weaker than those seen in the spectrum of HD 167402. Combined with the presence of a strong C III 1428 Å line and a very weak Si II 1264 Å line, the photospheric lines lead us to believe that HD 168941 has a spectral type near O9–B0. The strength of the N IV 1718 Å line supports the conclusion that HD 168941 has a spectral type near O9.5.

The Si IV wind profiles of HD 168941 are less developed than they are in a typical O9 II spectrum, but the C IV and N V

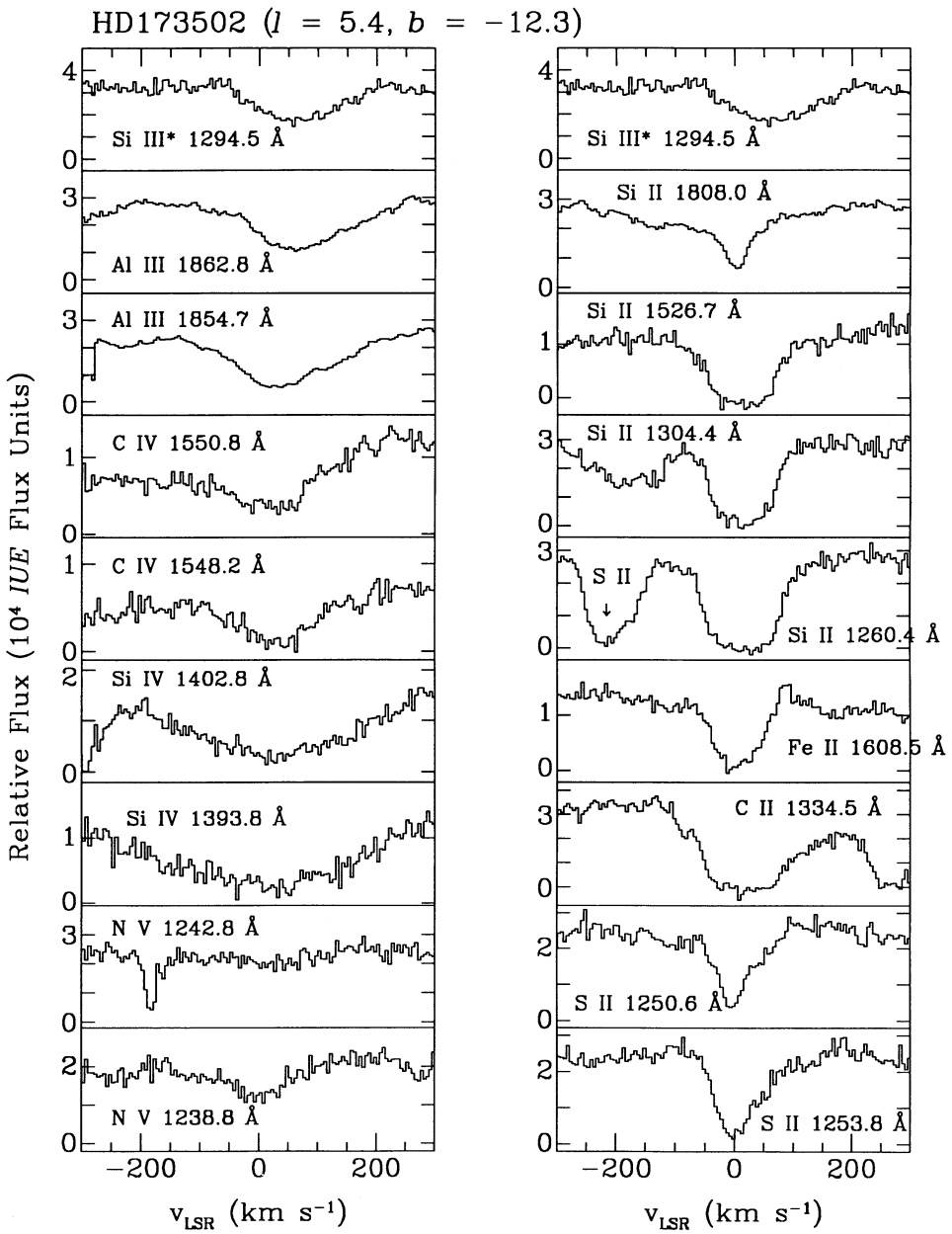

FIG. 4.—Selected interstellar absorption lines observed toward HD 173502, as in Fig. 1

profiles are similar to those of an O9 II star. The Si IV profiles are more indicative of a class III star at this spectral type. The photospheric Fe III lines near 1620 Å and 1925 Å also indicate that HD 168941 is at least a luminosity class III star.

Walborn (1982) classified HD 168941 as an O9.5 II–III star. Garrison et al. (1977) classified it O9.5 II-p, noting that the strength of the He II 4686 Å line is very strong and inconsistent with the rest of the spectrum. However, we find that the observed ultraviolet luminosity characteristics are appropriate for an O9.5–9.7 star with a luminosity class of II–III (similar to the classification given by Walborn 1982).

3.1.3. *HD 172140*

The spectrum of HD 172140 illustrates the spectral characteristics of a very early B giant. The Si III 1300 Å multiplet is intermediate in strength compared to the Si III multiplets seen in B0 and B1 stars. A weak N IV 1718 Å line suggests that the star may be somewhat cooler than B0. The presence of photospheric C IV and Si IV without associated wind profiles is representative of a class III star at these spectral types. In particular, more luminous stars have better developed C IV P Cygni profiles than those seen in HD 172140. The Si III 1417 Å line also indicates that the star must be more luminous than a class IV star but probably not as luminous as a Ib star. We classify HD 172140 as a B0.5 III star. This classification is identical to the optical classification assigned by Hill (1970).

3.1.4. *HD 173502*

HD 173502 has spectral features consistent with those exhibited by early B giants. The spectral characteristics are very similar to those of HD 172140 with the exception that the N IV 1718 Å line is slightly weaker relative to the Al II blend at

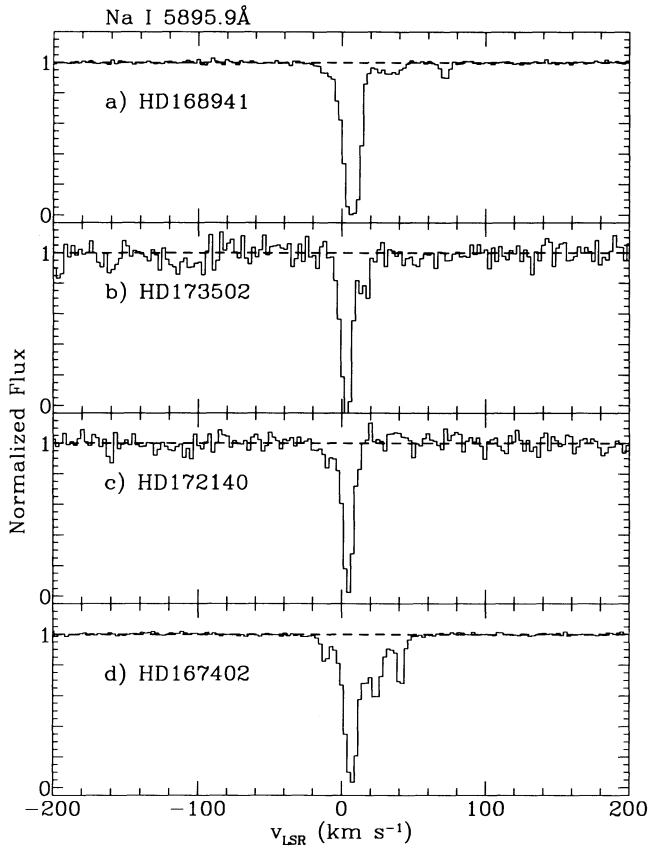

FIG. 5.—Normalized interstellar Na I 5889 Å absorption profiles observed toward (*a*) HD 168941, (*b*) HD 173502, (*c*) HD 172140, and (*d*) HD 167402 (from Sembach et al. 1992) are plotted against LSR velocity.

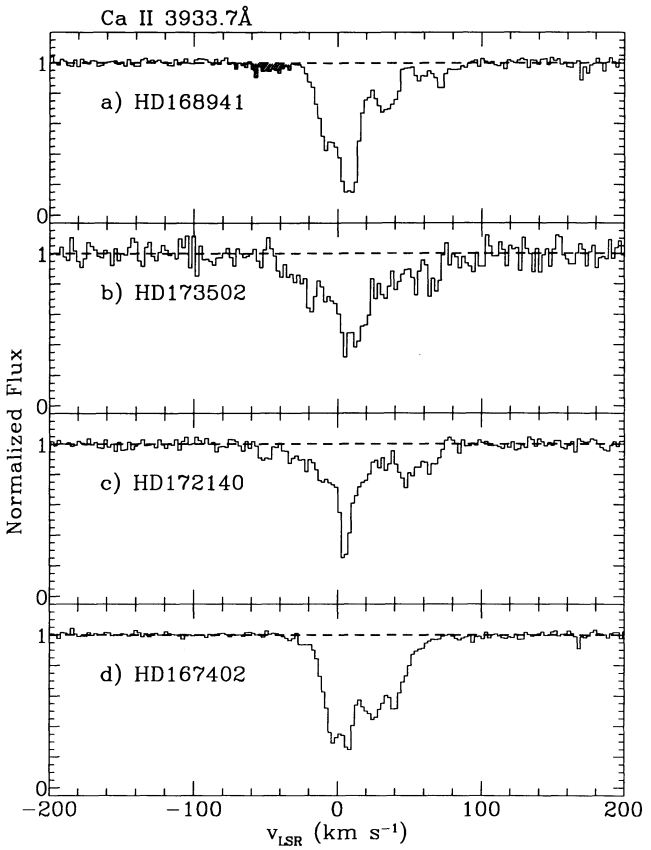

FIG. 6.—Normalized interstellar Ca II 3933 Å absorption profiles observed toward (*a*) HD 168941, (*b*) HD 173502, (*c*) HD 172140, and (*d*) HD 167402 (from Sembach et al. 1993) are plotted against LSR velocity. The broad shallow feature in the spectrum of HD 168941 (discussed in the text) is shaded. This resolved broad shallow absorption line cannot be attributed to Galactic rotation; the absorption occurs entirely at forbidden velocities.

1720 Å. HD 173502 was classified B1 II by Garrison et al. (1977). We assign a classification of B0.5 III based upon the ultraviolet stellar spectrum.

3.1.5. *Classification Summary*

We have assigned spectral/luminosity classifications to the four stars of interest in this study (see Table 2). These classifications are within half a subtype of the MK classifications cited in the literature. Given our assigned classifications, we derive the spectroscopic and vertical (z) distances listed in Table 2 using the O and B star absolute magnitude calibration of Walborn (1972, 1973) and the intrinsic colors of Johnson (1963). We have assumed a standard extinction—reddening relation for the diffuse ISM: $A_V = 3.1E(B-V)$. We estimate that the uncertainties of our distance estimations may be as large as $\pm 25\%$.

3.2. *Stellar Contamination*

A critical issue in the use of stellar targets for interstellar absorption studies is the degree of stellar contamination of interstellar lines superposed on stellar features. The uncertainty in continuum placement is a related issue because the level of the true continuum can be difficult to ascertain when interstellar absorption is blended with stellar photospheric, circumstellar, or wind lines.

Three of the four stars have large projected rotational velocities ($v \sin i \geq 75$ km s^{-1}) and/or large stellar radial velocities [$v_R(*) > 100$ km s^{-1}]. Both of these quantities are listed in Table 2. We have plotted the purely photospheric Si III* 1294 Å stellar absorption line in the top panels of Figures 1–4 so that the reader may visually compare the positions and line shapes of the interstellar and stellar absorption lines. The stellar radial velocities and projected rotational velocities of HD 168941, HD 172140, and HD 173502 are sufficiently large; in most cases the stellar and interstellar profiles can be distinguished. Nevertheless, the apparent interstellar profiles may contain a stellar absorption component, especially at large positive velocities. The HD 167402 stellar/interstellar blending is a more critical problem. The centroid of the stellar Si III* 1294 Å line is shifted $\sim +50$ km s^{-1} from the interstellar line centroids, but the rotational broadening of the stellar lines is not large. Many of the interstellar absorption profiles observed toward HD 167402 may be contaminated at positive velocities.

We have tried to select luminous stars that have relatively well-developed P Cygni profiles in the Si IV, C IV, and N V wind lines. Well-developed P Cygni profiles are advantageous for several reasons in addition to their usefulness for stellar classification (§ 3.1). Blending with stellar photospheric absorption is not a problem because the stellar absorption is smoothly spread out over hundreds of km s^{-1}, and a sufficiently developed wind provides a smoothly rising continuum. We show the C IV P Cygni profiles of HD 167402, HD 168941, HD 172140,

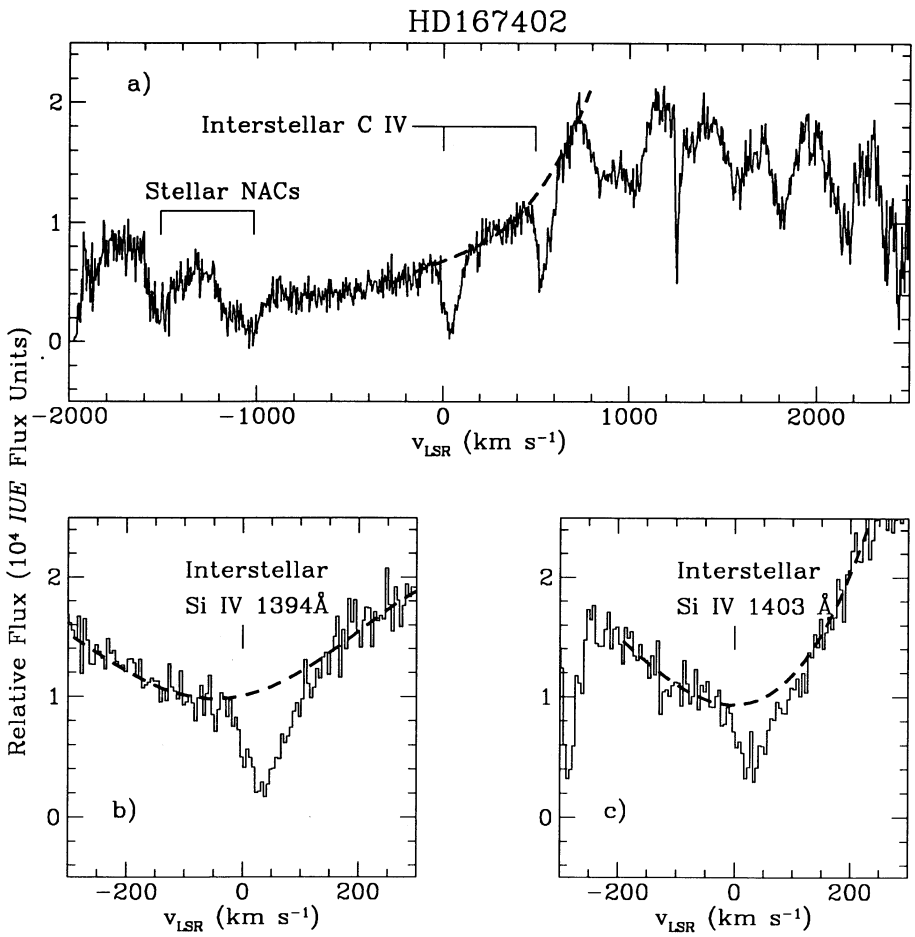

FIG. 7.—(*a*) The C IV P Cygni profile of HD 167402 in the LSR velocity frame of C IV 1548.2 Å. The interstellar C IV absorption lines and high velocity stellar narrow absorption components (NACs) are indicated, and the adopted continuum fit used to measure the equivalent widths and integrated column densities is shown with a heavy dashed line. Portions of the (*b*) Si IV 1393.8 Å and (*c*) Si IV 1402.8 Å profiles are shown, and the adopted continuum fits are again indicated with heavy dashed lines.

and HD 173502 in Figures 7–9. We have fit the continua of HD 167402 and HD 168941 (excluding velocity ranges containing interstellar absorption) with low order polynomials, and the resultant fits are indicated by heavy dashed lines in Figures 7 and 8. The C IV P Cygni profiles of HD 172140 and HD 173502 are not as well-developed as those of HD 167402 and HD 168941, so we have not attempted to fit continua to these wind lines (the continuum placement is too sensitive to the velocity ranges used for the fit).

We also show in Figures 7 and 8 portions of the Si IV 1394 and 1403 Å profiles observed toward HD 167402 and HD 168941. As noted in § 3.1, the Si IV P Cygni profiles of these stars are just beginning to develop, but we believe that the stellar continua are smooth enough to allow reliable continuum fits nevertheless. The polynomial fits that we adopt are again indicated by heavy dashed lines in Figures 7 and 8. The N V P Cygni profiles are also not well-developed, and the stellar continua are more difficult to fit than the Si IV stellar continua. Using the Si IV fits as a guide, we have attempted to fit the N V continua, but we consider the fits to be highly uncertain.

Hot star wind lines are known to contain temporally variable discrete narrow absorption components (NACs; e.g., Morton 1976; Snow 1977; Lamers, Gathier, & Snow 1982; Prinja & Howarth 1986). NACs have been detected in the P Cygni profiles of HD 167402 and HD 168941 (Prinja, Barlow, & Howarth 1990), and they are easily seen in Figures 7 and 8. The NACs are believed to have a stellar origin, and one might imagine "puffs" of matter which originate in the photosphere and are accelerated in the wind up to the terminal velocity (v_∞). If the puff model is correct, then the NACs are a potential source of interstellar absorption contamination. We do not believe that the NACs *directly* contaminate the interstellar absorption profiles presented in this paper for the following reasons: (1) NACs are observed to change significantly on hourly time scales, but they have almost always, until recently, been observed to occur at the same velocity with average central velocities of $0.8v_\infty$ (Snow 1977; Prinja & Howarth 1986; Prinja, Howarth, & Henrichs 1987). Since the terminal velocities of the HD 167402 and HD 168941 winds are, respectively, 2005 and 1755 km s^{-1} (Prinja et al. 1990), the expected velocities of the NACs are well-removed from the interstellar absorption features. However, Prinja et al. (1992) have recently presented *IUE* observations of discrete absorption features in the Si IV and N IV wind lines of ζ Pup that appear at -1000 km s^{-1} and then clearly migrate to larger negative velocities.

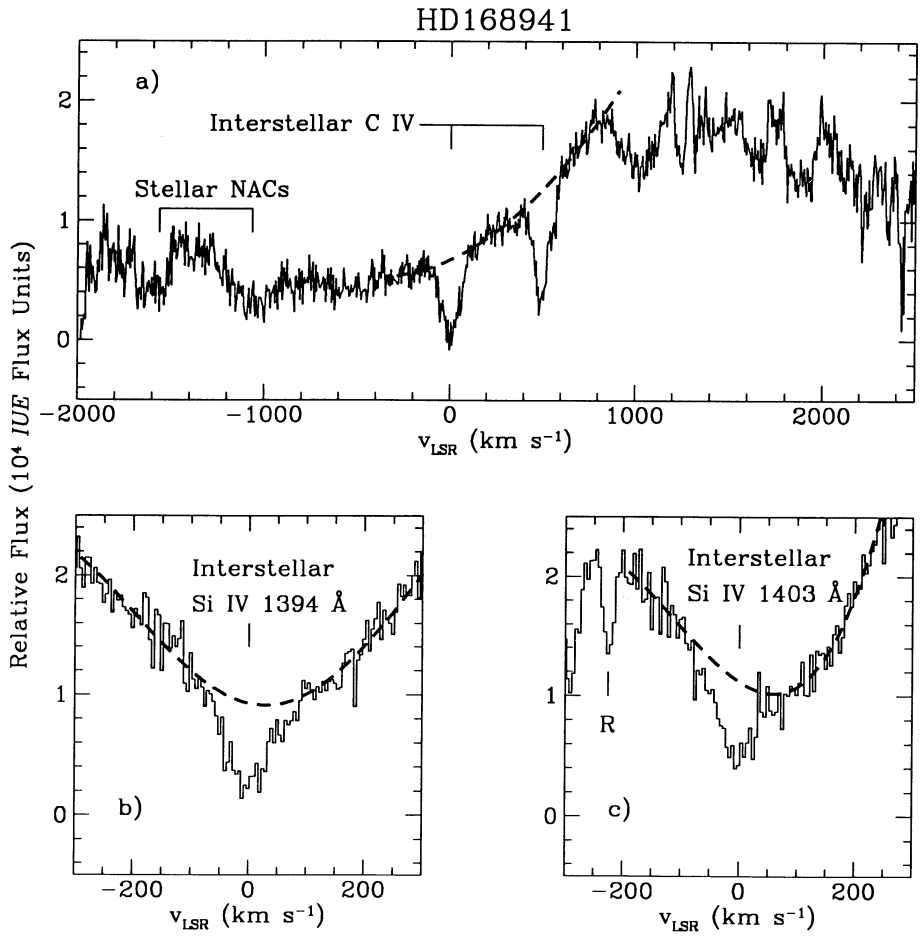

FIG. 8.—(*a*) C IV P Cygni profile of HD 168941 in the LSR velocity frame of C IV 1548.2 Å. As in Fig. 7, the continuum fit is indicated by a heavy dashed line. The continuum fits used for the (*b*) Si IV 1393.8 Å and (*c*) Si IV 1402.8 Å lines are shown with heavy dashed lines.

NACs that appear at ~ -1000 km s^{-1} in the C IV 1551 Å velocity frame are still roughly 500 km s^{-1} removed from the interstellar C IV 1548 Å line though. (2) Prinja (1988) and Prinja & Howarth (1988) have argued that the puff concept is not consistent with the observed behavior of NACs in the winds of four O stars. Based upon *IUE* observations of 68 Cyg, ξ Per, 19 Cep, and HD 162978, they find that low-velocity NACs predicted by the puff model are not observed. Instead, they find that broad low-velocity absorption enhancements appear at $\sim 0.55 v_\infty$ and evolve into the high-velocity NACs. The NACs observed in the ζ Pup wind lines also become increasing narrow as they migrate to increasingly negative velocities. Thus we conclude that the NACs are more likely to *indirectly* contaminate the interstellar absorption profiles by introducing continuum variability. HD 168941 was observed at three different times over the course of 7 years, and HD 167402 was observed at two different times during the same period. A small amount of continuum variability is clearly evident in the individual spectra, but it can be difficult to distinguish true variability from the shifting fixed pattern noise caused by the intentional target offsets (§ 2) and variability of the particle radiation-induced background. To assess the magnitude of this indirect contamination, we have measured the equivalent widths of the interstellar C IV absorption profiles in the individual spectra, and we find that the equivalent widths determined from the individual spectra agree with the equivalent widths determined from the combined spectra, within the uncertainty of the measurements. Furthermore, one might argue that the temporally averaged continuum that we obtain by combining the spectra is more appropriate for interstellar absorption studies.

Circumstellar H II regions are also a potential source of confusion. The four stars in this paper are also in the 40 star sample of Savage & Massa (1987) which was selected to avoid prominent H II region contamination. No obvious nebulosity is apparent on the Palomar sky survey prints containing HD 172140 and HD 173502. The Palomar sky survey fields containing HD 167402 and HD 168941 contain a considerable amount of nebulosity, but the sight lines do not pass through any obvious H II regions, filaments, or OB associations. Savage & Massa (1987) and Paper III point out that based upon the LTE calculations of Black et al. (1980) and Cowie, Taylor, & York (1981), the expected circumstellar column densities of Si IV, C IV, and N V for these stellar types are one to several orders of magnitude less than the observed column densities. However, if the stars are hotter and/or less luminous than we believe, then the column densities of circumstellar high ionization stages will be larger. Also, the non-LTE calculations of de Kool & de Jong (1985) predict somewhat higher column densities than Cowie, Taylor, & York (1981). The possible contri-

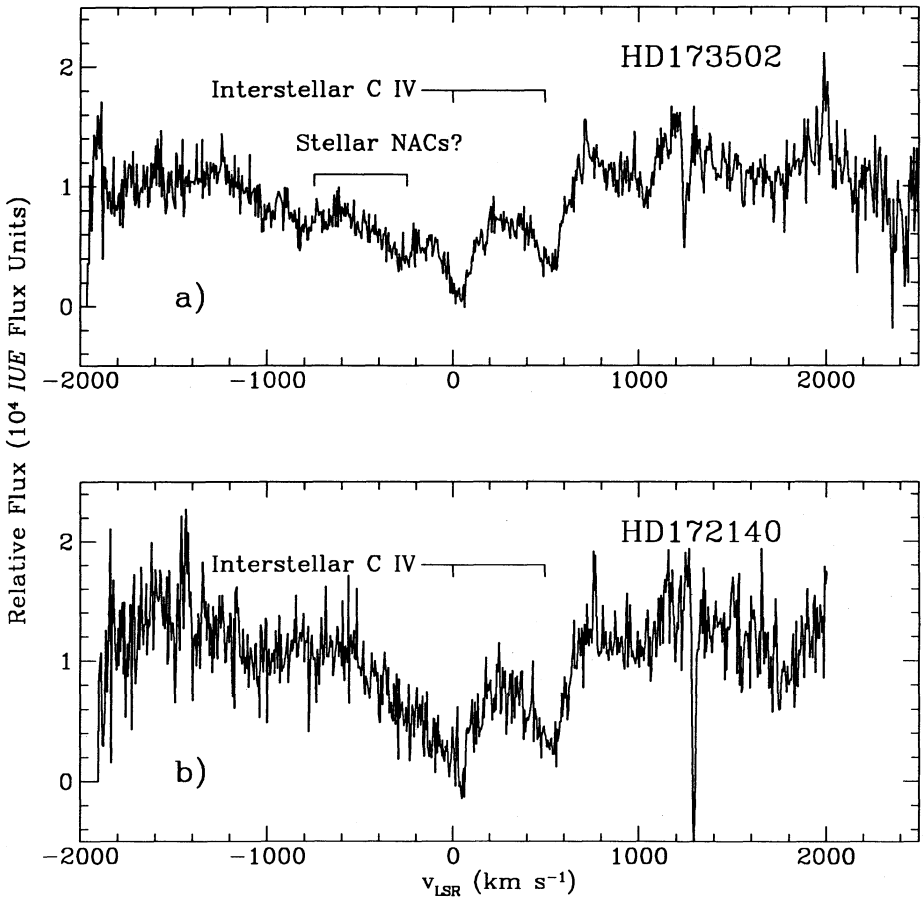

FIG. 9.—(*a*) The C IV P Cygni profile of HD 173502 in the LSR velocity frame of C IV 1548.2 Å. (*b*) The C IV P Cygni profile of HD 172140 in the LSR velocity frame of C IV 1548.2 Å.

bution of circumstellar H II regions to the observed absorption is important to bear in mind.

4. INTERSTELLAR ABSORPTION LINES

Selected interstellar absorption lines are plotted versus LSR velocity in Figures 1–4. The lines selected probe a wide range of densities and temperatures. High-density gas is traced by the Si II 1808 Å, Fe II 1608 Å, S II 1251 Å, and S II 1254 Å lines, and low-density gas is traced by the wings of the strong Si II 1527 Å, Si II 1304 Å, Si II 1260 Å, and C II 1335 Å lines (which are generally quite saturated in the core). Hot gas is traced by the Si IV, C IV, and N V doublets; the energies required to create these ions are 33.5, 47.9, and 77.5 eV, respectively.

4.1. *High Ion Column Densities*

Using the stellar continuum fits discussed in § 3.2, we have calculated the equivalent widths (W_λ) of the highly ionized interstellar absorption lines observed towards HD 167402 and HD 168941. These are listed in Table 3 along with the high ion column densities (see below) and integration ranges. Evaluation of the uncertainties in the equivalent widths is complicated. The *IUE* is not a photon counting instrument, and the noise is often dominated by fixed pattern noise. In addition, the uncertainty in the continuum placement and continuum variability must be accounted for.

We use the apparent optical depth technique described by Savage & Sembach (1991; see also Savage et al. 1989; Papers I–III, Savage et al. 1991, and Joseph & Jenkins 1991) to check for unresolved saturation in the high ion absorption profiles and to determine their column densities. We briefly review the procedure here and refer the reader to Savage & Sembach (1991) for details. The first step is to calculate the apparent optical depth per unit velocity, $\tau_a(v)$, using the usual relation

$$\tau_a(v) = \ln [I_c(v)/I_{obs}(v)] , \quad (1)$$

where $I_c(v)$ is the estimated continuum intensity and $I_{obs}(v)$ is the observed intensity at velocity v. The next step is to calculate the apparent column density per unit velocity, $N_a(v)$ [atoms cm^{-2} (km s^{-1})$^{-1}$], from the apparent optical depth

$$\log [N_a(v)] = \log \tau_a(v) - \log (f\lambda) + 14.576 , \quad (2)$$

where f is the oscillator strength and λ is the wavelength of the transition (in Å). Equation (2) follows from the relation between optical depth and column density

$$\tau(v) = \frac{\pi e^2}{m_e c^2} f\lambda N(v) , \quad (3)$$

The third step is to compare the $N_a(v)$ profiles of two doublet lines differing in the quantity $f\lambda$ (e.g., the C IV 1548 Å and the

TABLE 3

HIGH ION EQUIVALENT WIDTHS AND APPARENT COLUMN DENSITIES

Object	Ion	Wavelength (Å)	$W_\lambda \pm 1\,\sigma$ (mÅ)	Log N_a ($-1\,\sigma$)	Log N_a (cm^{-2})	Log N_a ($+1\,\sigma$)	Integration Range v_- (km s^{-1})	Integration Range v_+ (km s^{-1})
HD 167402.....	Si IV	1393.755	303 ± 32	13.68	13.72	13.76	−50	+150
		1402.770	189 ± 39	13.68	13.74	13.80	−50	+150
	C IV	1548.195	426 ± 37	14.19	14.28	14.36	−50	+150
		1550.770	286 ± 22	14.13	14.28	14.39	−50	+150
	N V[a]	1238.821	87 ± 26	13.56	13.67	13.75	−50	+150
		1242.804	52 ± 25	13.56	13.73	13.86	−50	+150
HD 168941.....	Si IV	1393.755	293 ± 46	13.67	13.71	13.76	−150	+100
		1402.770	167 ± 46	13.61	13.72	13.76	−150	+100
	C IV	1548.195	565 ± 41	...	>14.37	...	−150	+100
		1550.770	395 ± 26	14.44	14.46	14.49	−150	+100
	N V[a]	1238.821	192 ± 29	13.94	14.02	14.09	−150	+100

[a] Uncertainties may be larger than the estimated uncertainties listed in this table because continuum placement for measurement of the N V column densities is very ambiguous.

C IV 1551 Å lines). If the $N_a(v)$ profiles agree to within $\sim$0.1 dex, then the effects of unresolved saturated structure are not large; if the $N_a(v)$ profile of the stronger line lies significantly below that of the weaker line, then the profile contains significant unresolved saturated structure in the velocity ranges where the reliably measured profiles are discrepant. If no saturated structure is present, then the final step is to integrate across the line to obtain the total column density. The many advantages of this analysis technique are discussed by Savage & Sembach (1991). The primary advantage over the standard curve of growth analysis is that the velocity information in the absorption profiles is retained. In cases where the two techniques can be appropriately compared, they yield consistent results (Savage & Sembach 1991; Paper III). Comparison of high ion column densities derived with this method from *IUE* observations of HD 167756 (Paper III) to high ion column densities derived from higher resolution (FWHM = 3.5 km s^{-1}) *Hubble Space Telescope* spectra of HD 167756 (Savage, Sembach, & Cardelli 1993b) indicates that very accurate column densities can be obtained from *IUE* data.

The apparent column densities of the Si IV doublet at 1394 and 1403 Å and the C IV doublet at 1548 and 1551 Å are plotted versus LSR velocity in Figures 10 and 11 for HD 167402 and HD 168941, respectively. The corresponding column densities (integrated from v_- to v_+) are listed in Table 3. The weak member of each doublet is plotted with a solid line and the strong member is overplotted with a dashed line. In the wings, where the apparent column density is not well determined, the weak line profile is indicated by filled squares and the strong line by open squares. Error bars ($\pm 1\,\sigma$) for the weak line profile are plotted at the top of the panel while error bars for the strong line are plotted at the bottom. We also show the N V doublet at 1239 Å and 1243 Å in Figures 10*b* and 11*b*. Due to its intrinsic weakness, ambiguity of the continuum placement, and poor sensitivity of the *IUE* vidicon detector in that region, we were unable to confidently measure the apparent column density profile of the weak line of the N V doublet at 1243 Å observed toward HD 168941. We were unable to measure the apparent column density in the core of the C IV 1548 Å profile toward HD 168941 because the detected intensity is near zero. Finally, we overplot in Figures 10*d* and 11*d* the best Si IV, C IV, and N V apparent column density profiles in order to directly compare the shape of and structure in the profiles (§§ 4.2 and 7.1).

The Si IV apparent column density profiles are reasonably well determined and free of unresolved saturation. The Si IV profile toward HD 167402 is measurable and unsaturated over the range -10 km s^{-1} $\leq v_{\rm LSR} \leq +110$ km s^{-1}, and the Si IV profile toward HD 168941 is detected and unsaturated over the range -60 km s^{-1} $\leq v_{\rm LSR} \leq +25$ km s^{-1}. The C IV profiles toward HD 167402 are detected and unsaturated from $v_{\rm LSR} \approx -10$ km s^{-1} to $\approx +110$ km s^{-1} as well. Toward HD 168941, the strong line of the C IV doublet cannot be measured from ≈ -20 km s^{-1} to $+8$ km s^{-1}, but the profile is well-determined and unsaturated from ≈ -80 km s^{-1} to -20 km s^{-1} and from $\approx +8$ km s^{-1} to $+80$ km s^{-1}. However, the HD 168941 Si IV and C IV profiles have roughly the same shape, so the weak line of C IV probably is not seriously affected by unresolved saturated structure, and the total C IV apparent column density, integrated across the weak line, may be close to the actual value. The integrated N V column densities are quite uncertain. The placements of the N V stellar continua are ambiguous, and consequently the column density uncertainties may be larger than the uncertainties we have estimated and listed in Table 3 and Table 4 (below).

4.2. *Velocity Structure*

We concentrate on inner Galaxy stars ($2\overset{\circ}{.}3 \leq l \leq 5\overset{\circ}{.}8$) in order to minimize the effects of Galactic rotation and thereby improve our ability to search for radial inflow/outflow generated by spiral structure, fountains, chimneys, Galactic winds, or a bar in the Galactic center. For purposes of illustration, consider the following idealized treatment of Galactic rotation. If the rotation of the Galaxy is strictly circular, then the radial velocity (v_R) of a parcel of gas at longitude l, latitude b, and galactocentric radius R will be given by (see Mihalas & Binney 1981)

$$v_R = \sin l \cos b \left[\Theta(R) \frac{R_0}{R} - \Theta_0 \right], \quad (4)$$

where R_0 is the galactocentric radius of the Sun, Θ_0 is the linear rotation velocity of the Galaxy at R_0, and $\Theta(R)$ is the linear rotation velocity of the Galaxy at radius R. As l

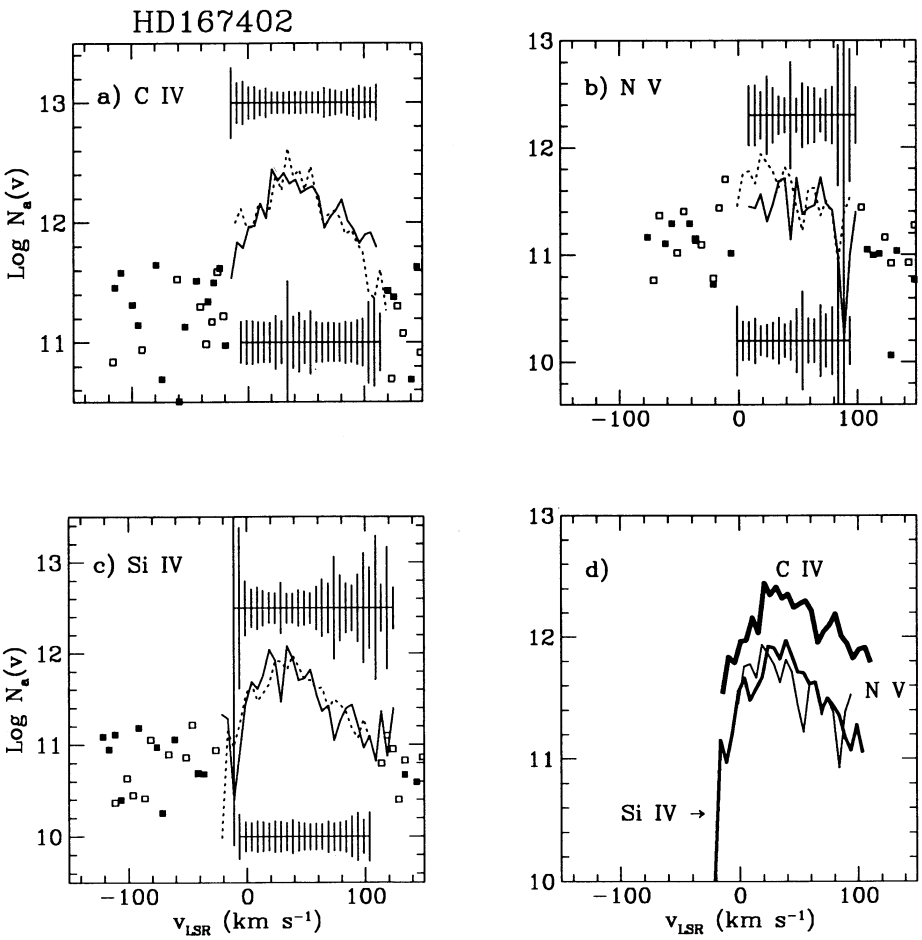

FIG. 10.—Logarithm of apparent column density [atoms cm^{-2} (km $s^{-1})^{-1}$] vs. LSR velocity (see § 4.1) observed toward HD 167402 for the (*a*) C IV doublet at 1548 and 1550 Å, (*b*) the N V doublet at 1239 Å and 1243 Å, and (*c*) the Si IV doublet at 1394 and 1403 Å. The weak member of each doublet is plotted with a solid line and the strong member is overplotted with a dashed line. At velocities where the apparent column density is not well determined, the weak line profile is indicated by filled squares and the strong line profile by open squares. Error bars ($\pm 1\ \sigma$) for the weak line profile are plotted at the top of each panel and error bars for the strong line are plotted at the bottom. (*d*) Overplot of the best N V (*thin line*), Si IV (*medium line*), and C IV (*heavy line*) apparent column density profiles.

approaches zero or b approaches 90°, v_R approaches zero. Consider a sight line through the first quadrant ($0° \leq l \leq 90°$). If the gas rotates on Keplerian orbits, then Θ will increase with decreasing R. When $R < R_0$, the gas will have a positive radial velocity. When $R > R_0$, the gas will have a negative radial velocity. Thus by observing interstellar absorption towards Galactic center stars, we also minimize kinematic ambiguity due to the uncertainty in the distance of the star. For example, if we observe a star in the first quadrant at $l \approx 5°$ and we estimate that the distance of the star is ~ 7 kpc, then we should only detect absorption at positive LSR velocities. Absorption at negative velocities due to Galactic rotation will not be detected unless the true distance to the star is more than twice the estimated distance. Since the uncertainties in the distances to the stars in Table 2 are typically $\pm 25\%$, negative velocity absorption cannot be attributed to the effects of Galactic rotation.

The interstellar gas in the Milky Way does not rotate on Keplerian orbits, but we arrive at the same conclusions when we use a measured rotation curve to calculate the expected velocities of the absorbing gas. The detailed intrinsic shape of an absorption profile depends on the gas velocity dispersion, the density distribution along the line-of-sight, the Galactic rotation curve, decoupling of halo rotation from disk rotation, and any sight line features that may affect the kinematics of the gas (e.g., an expanding spiral arm or superbubble). The observed profile also depends upon the instrumental spectral spread function. We have used the rotation curve obtained by Clemens (1985) to calculate the span of LSR radial velocities expected for the sight lines towards the four program stars, assuming the halo corotates with the underlying disk (we have also assumed that $R_0 = 8.5$ kpc and $\Theta_0 = 220$ km s^{-1}). These radial velocities are plotted versus line-of-sight distance in Figure 12. The expected radial velocity at the distance of the star, $v_R(d)$, is given in Table 2.

The most peculiar and intriguing aspect of the absorption profiles in Figures 1–4 is the significant amount of absorption at negative velocities. Consider the HD 168941 profile. From Figure 12 we see that the profiles are expected to extend from ~ 0 km s^{-1} to $\sim +50$ km s^{-1} if the halo/thick disk is perfectly corotating with the thin disk. However, the instrumental spread function and the gas velocity dispersion must be taken into account. If the radial velocity dispersion of the highly ionized gas is ~ 30 km s^{-1} and the spectral spread function of

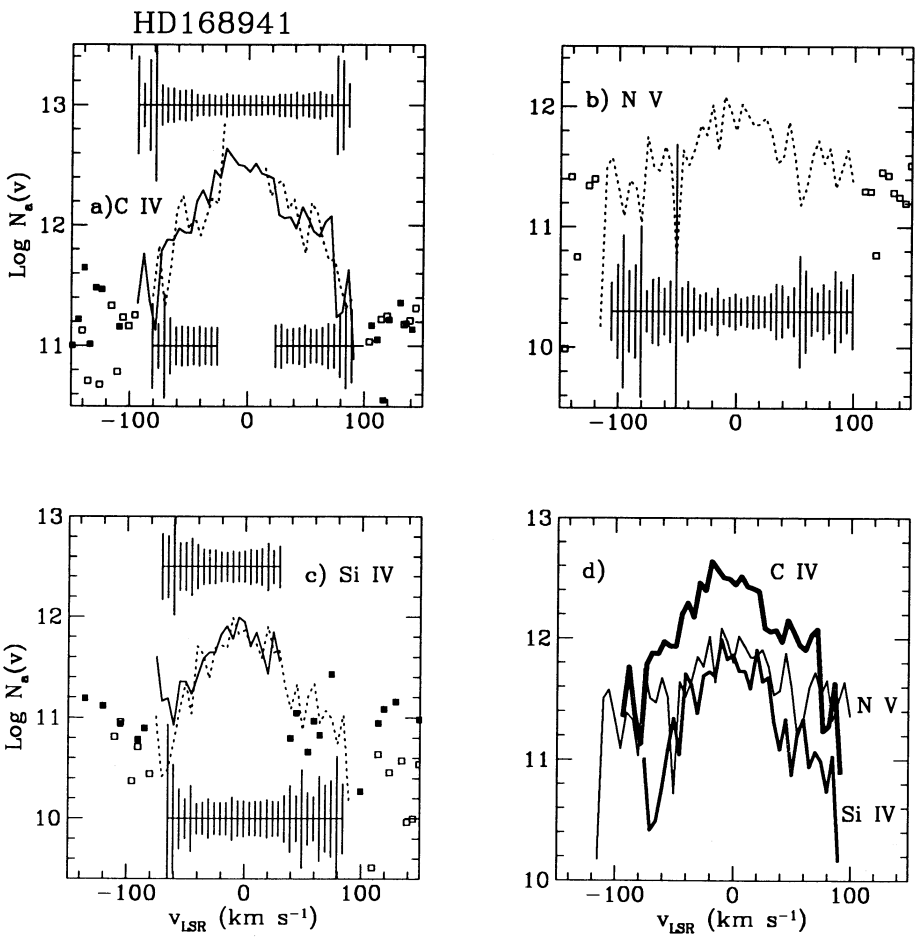

FIG. 11.—Logarithm of high ion apparent column densities [atoms cm^{-2} $(km\ s^{-1})^{-1}$] vs. LSR velocity observed toward HD 168941. See Fig. 10 caption for legend explanation.

the *IUE* is well described by a Gaussian with FWHM ~ 25 km s^{-1}, then the high ion profiles might be expected to extend from ~ -40 km s^{-1} to $\sim +80$ km s^{-1}. *However, the observed* C IV *profiles extend from* ~ -100 to $\sim +100$ km s^{-1}. The negative velocity extents of the Si IV and N V lines are more difficult to estimate because of the ambiguity of the continuum placement, but if we adopt the continuum fits shown in Figure 8, then the Si IV profiles extend from ~ -80 km s^{-1} to at least $+30$ km s^{-1}. Increasing the assumed distance of the star by 20% will not explain the negative velocity wing; if the true distance is 7.5 kpc instead of 6.3 kpc, then the profiles should extend from ~ -40 to $\sim +150$ km s^{-1}. The negative velocity absorption cannot be explained by decoupling halo corotation either. If the halo does not rotate at all, for example, inside of a galactocentric radius of 4 kpc, then the Solar motion toward HD 168941 will extend the absorption profile to ~ -20 km s^{-1} and the rotating disk gas probed by the first few kpc of the sight line will extend the profile to $\sim +20$ km s^{-1}; due to the gas velocity dispersion and instrumental broadening the absorption should be detected from ~ -60 to $+50$ km s^{-1}. Increasing the galactocentric radius of the nonrotating region only decreases the positive velocity extent of the profiles. Furthermore, based on analysis of 21 cm emission surveys, Lockman (1984) has concluded that H I in the inner Galaxy corotates up to at least 1000 pc from the plane. The low ionization gas lines with large oscillator strengths (e.g., C II 1334.5 Å, Si II 1260.4 Å) also show significant amounts of absorption at negative velocities, and the negative wings of these lines disappear into the continuum at the same velocity that the C IV lines disappear into the continuum (the velocity extent of the C IV absorption is indicated by vertical dashed lines in Fig. 2). The intermediate strength low ions (e.g., Si II 1304.4 Å, Si II 1526.7 Å) also show a negative velocity wing extending to about -100 km s^{-1}. The Na I optical doublet does not show any absorption beyond ~ -35 km s^{-1} (see Fig. 5), but the Ca II 3933 Å line shows a broad and very weak component extending from -35 km s^{-1} to -75 km s^{-1} (this broad weak absorption is shaded in Fig. 6). The signal-to-noise of the optical data is ~ 115 for the Na I profiles and ~ 45 for the Ca II profiles, so this weak broad feature is real. It is unlikely that this feature is stellar since the star has a large radial velocity as well as a large projected rotational velocity. We shall discuss some viable interpretations of this absorption at negative (i.e., forbidden) velocities in § 6.

This large amount of negative velocity absorption is not necessarily a universal feature of all Galactic center sight lines. The interstellar absorption observed toward HD 167402, which has nearly the same latitude as HD 168941 but is 3°.5 closer to the Galactic center in longitude (Table 2), extends from ~ -50 km s^{-1} to at least $+75$ km s^{-1}. From Figure 12 we see that the profiles toward HD 167402 are expected to extend from roughly -40 to $+70$ km s^{-1} (including instru-

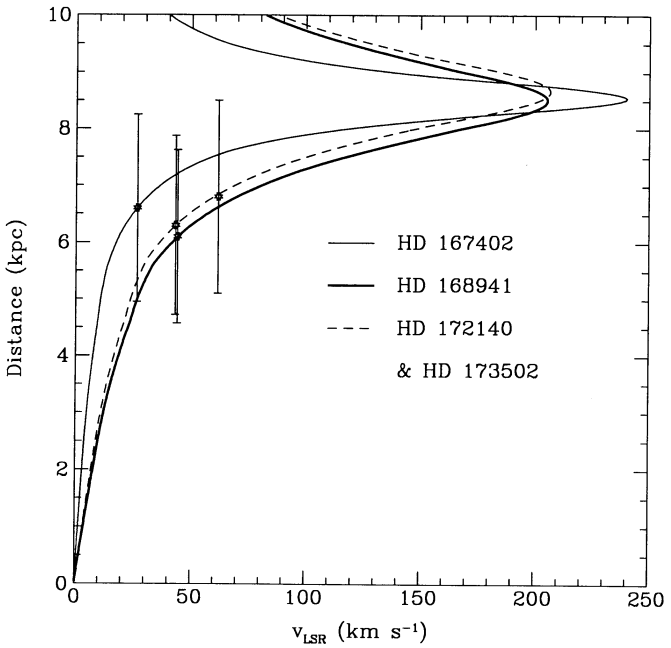

FIG. 12.—LSR radial velocities expected for gas towards the four inner Galaxy stars as a function of line-of-sight distance, assuming perfect corotation of the halo with the underlying disk. We have used the Galactic rotation curve obtained by Clemens (1985) for this calculation, and we have assumed R_0 = 8.5 kpc and Θ_0 = 220 km s^{-1}. The stars on each curve are placed at the line-of-sight stellar distance estimated in § 3.1 and listed in Table 2; the error bars indicate the 1 σ uncertainty in the estimated stellar distance.

mental broadening and the gas velocity dispersion). The observed high ion profiles extend from ~ -50 km s^{-1} to $+140$ km s^{-1}. In contrast to HD 168941, the HD 167402 profiles show only a small amount of absorption at forbidden negative velocities and a significant excess of absorption at large positive velocities. The strong low ion absorption lines are detected from ~ -50 km s^{-1} to $+140$ km s^{-1}, but the intermediate strength and weak low ions are clearly detected only from -50 to $+75$ km s^{-1}. The velocity extent of the C IV absorption is indicated by vertical dashed lines in Figure 1.

The high ion interstellar absorption profiles towards HD 172140 and HD 173502 are not as well determined as those toward HD 167402 and HD 168941 because the P Cygni profiles are not as well developed (see Fig. 9 and § 3.2) and the data quality of the few *IUE* spectra available for these stars is not as good as the data quality of the composite spectra of HD 167402 and HD 168941. However, the radial velocities of HD 172140 and HD 173502 (see Table 2) are large enough to distinguish stellar low ion absorption from interstellar absorption. The strong low ion profiles towards HD 172140 and HD 173502 show significant interstellar absorption out to -100 km s^{-1}, which is consistent with the HD 168941 data. Neutral sodium absorption is not detected at significantly negative velocities toward HD 172140 and HD 173502 (Fig. 5), but Ca II absorption is detected out to at least -60 km s^{-1} and may extend to -90 or -100 km s^{-1} toward HD 172140 and HD 173502 (Fig. 6). As noted by Danly et al. (1992), some structure is marginally resolved in the HD 172140 *IUE* profiles. The weak Si II 1808 Å, Fe II 1608.5 Å, and S II 1251 Å lines show two components, one centered on $\sim$0 km s^{-1} and the other centered on $\sim +50$ km s^{-1}. The *IUE* data are quite noisy, but traces of the $+50$ km s^{-1} component are possibly contained in some of the other profiles such as C IV 1548 Å or C II 1334.5 Å. The optical data are better-suited for studies of low ion component structure because the resolution and signal-to-noise are much better. The $+50$ km s^{-1} component is clearly detected in the Ca II profile (see Fig. 6).

The C II 1334.5 Å and C IV 1548.2 Å absorption profiles observed toward all four inner galaxy stars are compared in

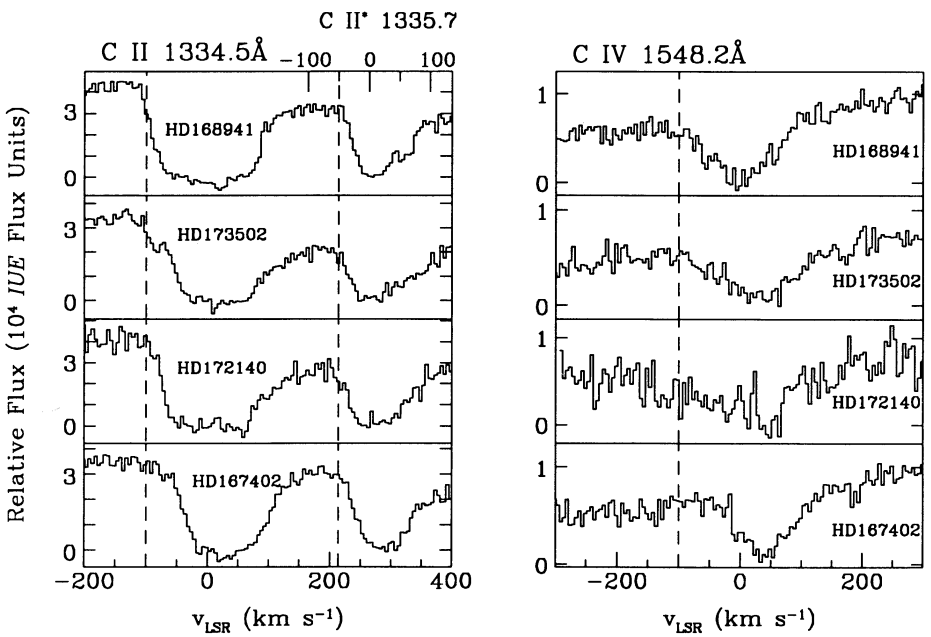

FIG. 13.—C II 1334.5 Å and C IV 1548.2 Å interstellar absorption profiles observed toward all four of the inner Galaxy stars, plotted in order of increasing sight line longitude from bottom to top. The C II* 1335.7 Å line appears in the C II 1334.5 panel from $+200$ km s^{-1} to $+400$ km s^{-1}; we have plotted the C II* LSR velocity scale on the top axis of the C II plot. For purposes of comparison, we have indicated -100 km s^{-1} in the LSR velocity frames of C II 1334.5 Å and C IV 1548.2 Å with a vertical dashed line, and we have indicated -50 km s^{-1} in the velocity frame of C II* 1335.7 Å also with a vertical dashed line.

Figure 13. The spectra are plotted in order of increasing sight line longitude from bottom to top. The C II* 1335.7 Å line appears in the C II 1334.5 Å profile from 200 to 400 km s^{-1}; we have plotted the C II* 1335.7 Å LSR velocity scale on the top axis of the plot. For purposes of comparison, we have indicated -100 km s^{-1} in the LSR velocity frames of C II 1334.5 Å and C IV 1548.2 Å by a vertical dashed line, and we have indicated -50 km s^{-1} in the velocity frame of C II* 1335.7 Å also by a vertical dashed line. The C II 1334.5 Å and C IV 1548.2 Å lines appear to extend to slightly greater negative velocities as the longitude increases while the negative wing of the C II* line does not appear to change much with sight line longitude. This suggests that the interstellar absorption at the highest negative velocities occurs in low-density gas (see § 7.2).

Curiously, the line profiles toward all four stars have very similar shapes, and the primary differences between them are that the centroid shifts to somewhat greater negative velocities with increasing longitude, and the HD 168941, HD 172140, and HD 173502 profiles are slightly broader than the HD 167402 profile. If the four sight lines all intersect a large expanding superstructure (e.g., the North Polar Spur supershell or the 3 kpc arm) or the same set of structures, then the absorbing gas on all four paths might have roughly the same temperature, turbulence, and bulk motion at a given radius, so one might expect the profiles to have more or less the same shape with the centroid shifts and breadth differences due to the slightly different viewing geometry for each sight line.

5. SIGHT LINE PROPERTIES

Danly et al. (1992) have obtained H I 21 cm emission profiles toward the four stars presented in this paper, and they find that H I 21 cm emission is detected at negative velocities toward all four stars out to ~ -100 km s^{-1}. Toward HD 168941 they also observe significant double-peaked H I emission between $+100$ and $+200$ km s^{-1} which has no counterpart in absorption. They attribute this emission to the inner galaxy feature J5 (Cohen 1975; Cohen & Davies 1976) and argue that its absence in absorption indicates that it is beyond the target star. There are several expanding H I features in the inner Galaxy near these sight lines (e.g., the 3 kpc arm, van der Kruit XII), and we discuss in the next section the possibility that the forbidden velocity gas we detect in low and high ion absorption is associated with these features. The H I column densities and average sight line densities based on the Lyman-α absorption measurements of Diplas & Savage (1993) are listed in Table 2. The four sight lines are characterized by low values of the average number density of neutral hydrogen. The integrated H I column densities observed toward HD 172140 and HD 173502 differ by 0.12 dex (32%) even though the stars are close together in the sky, while HD 168941 and HD 172140 have similar H I column densities, as do HD 167402 and HD 173502.

All four sight lines pass over the Sagittarius spiral arm and the 3 kpc arm (Courtes 1972; Oort 1977). All four sight lines also pass through or nearly through Galactic H I worm candidates in the catalog of Koo, Heiles, & Reach (1992). The sight line toward HD 167402 pierces Galactic worm candidate GW 0.5 $-$ 5.9 while the sight lines toward HD 168941, HD 172140, and HD 173502 pass near GW 6.5 $-$ 3.7, GW 5.1 $-$ 8.1 and GW 4.6 $-$ 3.1 (see Fig. 2 in Koo et al. 1992). If these Galactic worms are the cool walls of a chimney or bubble, then the forbidden velocity gas we detect in absorption may arise in the "turbulent mixing layers" proposed by Begelman & Fabian (1990) or in hot gas flowing up out of the chimney. We discuss these possibilities further in § 6.4.

The recent complete high-velocity cloud (HVC) catalog of Wakker & van Woerden (1991) identifies a HVC in the vicinity of our inner Galaxy sight lines. This object, which was originally detected by Saraber & Shane (1974), is centered on $l = 8°$ and $b = -4°$, has an angular extent of roughly 3°, and has a LSR velocity of ≈ -215 km s^{-1}.

6. KINEMATICS

The subject of interstellar absorption at velocities forbidden by Galactic corotation is not new. Based upon Copernicus observations of interstellar N I, N II, and Si III absorption on 47 sight lines, Cowie & York (1978) concluded that "gas motion at the highest velocities is not predominantly due to Galactic rotation." On the other hand, Lockman (1991) states that "it is now generally recognized that most Galactic H I (at least in the inner Galaxy) is in cylindrical rotation (or "corotation"), i.e., its velocity is overwhelmingly rotational and the rotational velocity does not change with z." Ostensibly, the kinematic behavior of gas traced by H I is inconsistent with the behavior of gas traced by heavier neutrals and ions commonly observed in the ISM. However, the inner Galaxy (especially the inner 3 or 4 kpc) is a complicated place, and these statements are probably both correct and even consistent in context. The stars in the Cowie & York (1978) sample are less than 3 kpc away, so Galactic rotation effects are not large and the profile widths are dominated by the gas velocity dispersion (and the motions of Gould's belt may introduce further confusion; see Lindblad 1974; Weaver 1974). In a recent review, Burton (1992) agrees that outside of the bulge (i.e., beyond the innermost few kpc), the Galaxy is essentially circularly rotating, but in the bulge region expansion as well as rotation components must be included to understand the observed gas motions. In this section we discuss our measurements in the context of the literature on interstellar gas detected at anomalous velocities and we offer a few plausible interpretations of the observed UV absorption.

6.1. *Previous Results*

The existence of gas flowing away from the Galactic center at intermediate to high forbidden velocities has been known for a long time; two of the most well-known expanding features in the inner Galaxy are the 3 kpc arm and the $+135$ km s^{-1} arm (Oort 1977, and references therein). Several other expanding features have been observed within $\pm 10°$ in l and b of the Galactic center with forbidden radial velocities ranging from roughly -200 km s^{-1} to $+150$ km s^{-1} (see Table 2 in Oort 1977; van der Kruit 1970; Sanders, Wrixon, & Penzias 1972; Saraber & Shane 1974; Cohen 1975; Cohen & Davies 1976). These structures were generally discovered in H I studies, but they have also been detected in CO observations (e.g., Bania 1980). They were also initially observed in the plane of the Galaxy, but early surveys soon revealed forbidden velocity objects hundreds of parsecs from the plane (Oort 1977). The negative velocity absorption presented in this paper may be associated with these objects. If so, then the *IUE* data provide interesting new information on the ionization and distances of the expanding features.

The existence of forbidden velocity gas (not including the traditional high-velocity clouds) at high Galactic latitudes has also been known for some time. In a study of Ti II, Ca II, and Na I optical absorption and H I 21 cm emission observed

toward nine pairs of aligned high-latitude foreground disk and distant halo stars, Albert (1983) finds that "the interstellar Ti II and Ca II observed toward all of these stars exhibit large peculiar velocities with respect to a corotating halo." She also finds that "toward the high-z star of each pair, an average of 69% of the total H I emission is produced by gas at velocities outside the corotation range." H I emission can be confusing due to emission from very distant gas, but ultraviolet interstellar absorption surveys corroborate Albert's conclusions. For example, Savage & Massa (1987) find that while interstellar absorption on disk sight lines does occur at the expected corotation velocities, absorption on lower halo sight lines does not. Danly et al. (1992) find that interstellar absorption toward stars less than a kiloparsec from the plane exhibits some peculiar velocity absorption, but the deviations from corotation rarely exceed 40 km s^{-1} (consistent with Cowie & York 1978), while interstellar absorption observed towards stars more than a kiloparsec from the disk frequently deviates from corotation by more than 40 km s^{-1}.

The velocity structures in many of the interstellar absorption profiles studied in Papers I–III are surprising as well. For example, the profiles toward HD 163522 are expected to extend from roughly -170 to 0 km s^{-1} assuming pure corotation of disk and halo gas (not including the effects of instrumental broadening and gas velocity dispersion; see Fig. 6 in Paper I), but the observed high ionization stage profiles extend from ~ -110 to $+60$ km s^{-1}. In some cases the observed anomalous profiles can be explained in terms of decoupling halo rotation and/or absence of gas in the inner Galaxy, but evidence of forbidden velocity gas is accumulating. Nonrotational components may play an important role in the kinematics of the Galaxy, especially in the bulge and halo.

6.2. *Flows Associated with Spiral Arms*

Perhaps the most plausible interpretation of the forbidden velocity gas we have detected is that the absorption occurs in outflowing or turbulent gas associated with spiral arms, especially the 3 kpc arm. Assuming the galactocentric distance of the 3 kpc arm is $\sim$3.5 kpc, the sight lines to HD 167402 and HD 168941 pass over the arm at $z \approx -560$ pc, the sight line to HD 172140 passes over the arm at $z \approx -930$ pc, and the sight line to HD 173502 passes over the arm at $z \approx -1080$ pc. Discovery of the 3 kpc arm motivated Moore & Spiegel (1968) to explore the dynamics of gas flowing out of the inner Galaxy with outward velocities of $\sim$50 km s^{-1}, and they argue that a shock must form in the outflowing gas. They further argue that hydrostatic equilibrium will break down behind this shock, and the resultant vertical pressure gradients will turbulently drive gas motions away from the plane leading to an increase in the scale height of the gas. This increase in the scale height of the gas has been recently confirmed by studies of the response of the gaseous thick disk to spiral and other wave perturbations by Martos & Cox (1993); the numerical two-dimensional and three-dimensional magnetohydrodynamic simulations of nonlinear Galactic gas flows carried out by Martos & Cox (1993) indicate that the kinematics of gas flows are complex with rising and falling motions above spiral arms and radial inward and outward accelerations of the gas superposed on Galactic rotation. Furthermore, Martos & Cox (1993) find that the amplitude of the wave motion increases with the height z above the midplane reaching velocities on the order of several times 10 km s^{-1} well within $z = 1$ kpc in both radial and vertical directions. Thus these simulations *predict* the forbidden velocity gas we detect in absorption. These motions might not be easily detectable when the sight lines pass the Sagittarius arm because of the z-dependence, but they should be detectable in the vicinity of the 3 kpc arm. If magnetic fields are ignored, Martos & Cox (1993) find that the vertical and outward velocities can be much larger. The H I maps from Burton (1985) indicate that the 3 kpc arm is moderately confined to the disk, but this is not inconsistent with the model of Martos & Cox (1993) because the rising gas is likely to be turbulent and the hydrogen could be mostly ionized before it reaches large z distances.

6.3. *Motions Associated with a Galactic Bar*

Forbidden velocity gas in the inner Galaxy can also be explained by hypothesizing that there is a bar in the Galactic center. Various authors (e.g., de Vaucouleurs 1964; Blitz & Spergel 1991; Binney et al. 1991; Weinberg 1992) have suggested that there is evidence that our Galaxy is barred. Binney et al. (1991) have shown that closed orbits produced in the gravitational potential of a Galactic bar can lead to gas with velocities that are forbidden to circular orbits in an axisymmetric potential. The maximum forbidden velocity at a given longitude depends on the exact form of the potential and the viewing angle of the bar. Since these parameters are not yet established, it is difficult to quantitatively compare the forbidden velocities we detect to those predicted by the bar hypothesis. The fact that the absorption profiles appear smooth at forbidden velocities is consistent with this explanation, but higher resolution observations of these sight lines are needed to determine if the profiles are intrinsically smooth.

6.4. *Fountains and Chimneys*

We originally initiated this research in order to search for global radial inflow which might be generated by a hot Galactic fountain. For example, Bregman (1980a) has suggested that hot Galactic fountain gas ($T_0 \approx 10^6$ K at $z = 0$ kpc) will move from its point of origin in the disk buoyantly upward and radially outward (due to an assumed radial pressure gradient at the base of the fountain and a decrease of the radial gravitational force with height versus constant centrifugal force) before thermal instabilities cause clouds to form in the fountain flow. The pressure in the halo cannot support the clouds, so after formation they fall radially inward and ballistically return to the galactocentric radius from which they started. Therefore the fountain gas should show global motion away from the plane and away from the Galactic center or motion toward the plane and toward the Galactic center, depending upon which phase of the fountain cycle is being probed. This model qualitatively explains the motions of the high-velocity clouds (see Wakker 1991, and references therein); some of the HVCs could be cool clouds falling back towards the disk in the returning phase of the fountain, and consequently they are detected at high Galactic latitudes with high negative velocities with respect to the local standard of rest. One might expect highly ionized gas to exhibit motion which is different from the motion of low-ionization gas since the ions might exist in different phases of the fountain. Radially inflowing gas should produce excess interstellar absorption at positive LSR velocities. We do not detect overwhelming evidence of inflowing gas; comparison of the expected LSR velocities (Fig. 12) to the observed absorption profiles (see Figs. 1–4, 10, and 11) shows no obvious excess absorption at positive velocities. Only the HD 167402 high ion absorption profiles show significant

amounts of absorption beyond the estimated radial velocity at the distance of the star, $v_R(d)$ [see Table 2]. However, we do not consider this absence of inflowing gas to be strong evidence against the Galactic fountain theory. One can think of many reasons that radial inflow might not occur in the fountain cycle. The presence of a thick disk of gas may stifle radial inflow if the thick disk drag is greater than the gravitational force. Pressure from magnetic fields and cosmic rays may also help balance the gravitational force. If the fountain gas is initially cooler ($T_0 = 3 \times 10^5$ K instead of $T_0 = 10^6$ K), as required by Houck & Bregman (1990) to reproduce the 1 kpc scale height neutral interstellar gas, then it will not flow as far from the plane and radial motions may be greatly diminished. Furthermore, in a cool fountain the high ions may exist in the *outflowing* phase of the fountain, and a cooler fountain may thus provide a viable explanation of the negative velocity absorption observed toward HD 168941, HD 172140, and HD 173502.

Based upon the ideas proposed by Begelman & Fabian (1990), Slavin, Shull, & Begelman (1993) have suggested that the column densities of interstellar C IV, N V, and Si IV observed in absorption could be produced in "turbulent mixing layers" between hot gas inside bubbles or chimneys and the cooler neighboring ISM (i.e., the bounding walls of the bubble or chimney). Chimney walls would tend to prevent radial motions, but if the superstructure is expanding rapidly enough or if the turbulent mixing layer has a large gas velocity dispersion, then absorption at high forbidden velocities might be expected. The most obvious superstructure that these sight lines might pass through is the North Polar Spur (Radio Loop I). The boundaries of this superstructure are somewhat difficult to determine near the plane, but Berkhuijsen, Haslam, & Salter (1971) have fit the radio continuum loop with a small circle centered on $l = 329°$ and $b = 17.^\circ5$ with a diameter of 116°, so these sight lines may indeed pierce the object. According to Heiles (1984), the NPS is centered on $l = 331°$ and $b = 14°$ and has a diameter of 120°. Furthermore, the North Polar Spur (NPS) may contain significant amounts of Si IV, C IV, and N V; Burks et al. (1991) and Savage et al. (1993a) have suggested that much of the high ion interstellar absorption observed on the 3C 273 sight line may be associated with the NPS. The NPS isn't expanding rapidly enough to explain the negative velocity absorption discussed in this paper (Heiles 1984 finds that the NPS is expanding at ~ 25 km s^{-1}), but Iwan (1980) has argued that the Radio Loop I and the X-ray emission inside of Loop I cannot be understood in terms of a single supernova remnant model, and therefore the cavity blown out by the SN that generated Loop I must have been "reheated" by the shock from a more recent SN remnant. Loop IV is a likely candidate for the reheating SN remnant. Gas from the younger SN remnant may be expanding into the Loop I cavity at several hundred km s^{-1} and could plausibly have a radial component between -50 and -100 km s^{-1} in the direction of HD 168941. The principal weakness with this hypothesis is that Loop IV is a considerable distance from our inner Galaxy sight lines and consequently the younger SN remnant must still be expanding at several hundred km s^{-1} after traveling through several hundred parsecs of the Galaxy including the plane. This may not be a problem if the Loop I SN remnant thoroughly evacuated this region in advance of the Loop IV SN remnant.

We noted in § 5 that these sight lines pass near Galactic worm candidates identified by Koo et al. (1992). Inspection of Figure 2 in Koo et al. (1992) suggests that these worms may be the walls of a chimney: GW 4.6−3.1, GW 5.1−8.1, and GW 6.5−3.7 have the appearance of a wall at $l = 5°$ extending contiguously from the plane up to $b \approx -9°$, and GW 0.5−5.9 has the appearance of a wall on the opposite side of the chimney at $l \approx 0°$ extending from the plane up to $\approx -9°$. Koo et al. place these "walls" at significantly different distances. However, the worms are near $l = 0°$ and have low velocities, and therefore the kinematic distance estimates are highly uncertain. If these worms are indeed walls of a chimney, then turbulent mixing layers once again become an interesting potential explanation of the forbidden velocity gas we detect with the *IUE*. Slavin et al. (1993) find that turbulent mixing layers tend to be at least partially underionized, so the high ionization stages that we detect may exist in a gas with a significantly higher velocity dispersion than 30 km s^{-1} leading to the detection of interstellar absorption at intermediate to high negative velocities.

However, it is worth noting that Cox (1991) has argued, based on evidence that the Milky Way has a thick disk coupled with new results showing that a magnetic field parallel to the disk can inhibit the blow-out of a supernova bubble (Shapiro 1991; Tomisaka 1991) that the fountain/chimney models are less tenable than originally thought.

6.5. *Inner Galaxy Wind*

Bregman (1980b) has hypothesized that gas lost from bulge stars may be supernova-heated sufficiently to drive a wind out the poles of the bulge. This idea is apparently consistent with the H I distribution in the inner 3 kpc of the Galaxy; Lockman (1984) finds that inside 3 kpc, 90% of the H I is within a few hundred parsecs from the plane. Perhaps the H I above 400 pc has been removed by a wind. The absorption at negative velocities presented in this paper could be associated with a bulge wind, but since only a small amount of negative velocity gas is observed toward HD 167402, some explanation for the lack of wind in that direction must be conceived. One possible explanation is that HD 167402 is somewhat closer than we think it is, and consequently the HD 167402 sight line does not extend far enough into the inner Galaxy to pierce the region where the wind is blowing. However, if HD 167402 is closer, then the excess positive velocity absorption from $\sim +40$ to $\sim +150$ km s^{-1} becomes more interesting. As noted in § 3.2, for some of the ions this excess positive velocity absorption may be stellar contamination, but in the case of C IV, the positive velocity interstellar absorption to $\sim +110$ km s^{-1} is clearly detected against the smooth P Cygni profile.

7. PHYSICAL CONDITIONS AND IONIZATION

7.1. *High Ions*

Perhaps the most important result of this series of papers is the frequent detection of N V in absorption. The observed column densities of this ion are difficult to produce in warm photoionized halo models, so the existence of N V probably reveals the presence of collisionally ionized gas. Furthermore, the gas is probably hot. In collisional ionization equilibrium, the N V ionization fraction peaks at 2×10^5 K (Shapiro & Moore 1976); however, Edgar & Chevalier (1986) have found that collisionally ionized cooling fountain gas can be overionized so that N V could exist at lower temperatures. The calculations of Edgar & Chevalier (1986) appear to reproduce the correct column densities of C IV and N V but fall short of the

TABLE 4

FINAL HIGH ION COLUMN DENSITIES AND RATIOS

OBJECT	log N(Si IV) (cm^{-2})	log N(C IV) (cm^{-2})	log N(N V)[a] (cm^{-2})	$\frac{N(\text{C IV})}{N(\text{Si IV})}$	$\frac{N(\text{C IV})}{N(\text{N V})}$	INTEGRATION RANGE v_- (km s^{-1})	INTEGRATION RANGE v_+ (km s^{-1})
HD 167402	$13.74^{+0.06}_{-0.06}$	$14.28^{+0.11}_{-0.15}$	$13.67^{+0.08}_{-0.11}$	3.4 ± 1.1	4.0 ± 1.5	-50	$+150$
HD 168941	$13.72^{+0.04}_{-0.05}$	$14.46^{+0.03}_{-0.02}$	$14.02^{+0.07}_{-0.08}$	5.5 ± 0.7	2.8 ± 0.5	-150	$+100$
	$13.65^{+0.04}_{-0.04}$	$14.25^{+0.02}_{-0.02}$	$13.72^{+0.04}_{-0.05}$	4.0 ± 0.4	3.4 ± 0.4	-40	$+30$
Galactic average[b]	...	...	...	3.6 ± 1.3	4.6 ± 2.7	...	...

[a] Continuum placement for measurement of the N V column density is very ambiguous; consequently, uncertainties in this column density may be greater than the formal estimates given in this table.

[b] From Paper III.

observed Si IV column density by a factor of 4 or 5. On the other hand, photoionization calculations (e.g., Hartquist, Pettini, & Tallant 1984; Fransson & Chevalier 1985; Bregman & Harrington 1986) predict the observed Si IV and C IV column densities but have difficulty explaining the frequent detection and observed column densities of N V. The observed high ion column densities appear to require composite models such as the self-ionizing fountain proposed by Shapiro & Benjamin (1991) or self-ionizing turbulent mixing layers (Slavin et al. 1993).

The observed high ion column density ratios are surprisingly constant and independent of z (Pettini & West 1982; Paper III). The average high ion column density ratios from Paper III are $\langle N(\text{C IV})/N(\text{Si IV})\rangle = 3.6 \pm 1.3$ and $\langle N(\text{C IV})/N(\text{N V})\rangle = 4.6 \pm 2.7$. Our best estimations of the high ion column densities and the measurable high ion column density ratios observed toward HD 167402 and HD 168941 are listed in Table 4. The C IV to N V ratios observed towards both stars are within one sigma of the mean from Paper III. The C IV to Si IV ratio observed toward HD 167402 is close to the mean from Paper III, but toward HD 168941 it is more than 1 σ larger than the mean. Some of the gas on the HD 168941 sight line may be more highly ionized than the average sight line from Paper III in the sense that there is more N V and less Si IV than average. We also show in Table 4 the high ion ratios observed towards HD 168941 integrated over the core only (from -40 to $+30$ km s^{-1}). These core high ion ratios are closer to the mean ratios obtained in Paper III, which suggests that intermediate and high velocity gas is more highly ionized on this sight line; this is also evident in Figure 11*d*. Changing degrees of ionization as a function of LSR velocity can be determined directly from the apparent column density plots in Figures 10*d* and 11*d*. In Figure 10*d*, for example, we see that toward HD 167402, the C IV column density is $\sim$0.5 dex higher than the Si IV and N V column densities at LSR velocities greater than $\sim +20$ km s^{-1}, while it is only 0.2 to 0.4 dex higher between 0 and $+20$ km s^{-1}. The Si IV and N V column densities are comparable across most of the measured column density profile. Toward HD 168941 (Fig. 11*d*), the Si IV and N V column densities are comparable between -40 and $+30$ km s^{-1} and lie roughly 0.5 dex below the C IV column density. At $|v_{\rm LSR}| > 40$ km s^{-1}, the C IV and Si IV column densities fall off more rapidly than the N V column density. However, these changing ionization trends are only marginally detected since the error bars generally grow larger at intermediate and high velocities.

7.2. *Low Ions*

The C II* line shown in Figure 13 is a density diagnostic (the C II* 1335.7 Å line arises from the $(2s^2 2p)\ ^2P^o_{3/2}$ excited fine structure level of the ground state). Assuming the gas is in statistical equilibrium (i.e., $dn/dt = 0$), one can show (see Spitzer 1978) that the ratio of the number density of atoms in the $(2s^2 2p)\ ^2P^o_{3/2}$ level (n_2) to the number density of atoms in the $(2s^2 2p)\ ^2P^o_{1/2}$ level (n_1) is

$$\frac{n_2}{n_1} = \frac{n_e \gamma_{12}(e) + n_{\rm H\ I} \gamma_{12}(\text{H I})}{A_{21} + n_e \gamma_{21}(e) + n_{\rm H\ I} \gamma_{21}(\text{H I})}, \quad (5)$$

where n_e is the free electron number density, $n_{\rm H\ I}$ is the neutral hydrogen number density, $\gamma_{12}(e)$ and $\gamma_{12}(\text{H I})$ are, respectively, the rate coefficients for excitation by collisions with electrons and neutral hydrogen, $\gamma_{21}(e)$ and $\gamma_{21}(\text{H I})$ are the rate coefficients for de-excitation by collisions with electrons and neutral hydrogen, and A_{21} is the transition probability for spontaneous radiative decay. The electron collision rate coefficients are proportional to the collision strength (Spitzer 1978); we use the effective collision strength calculated by Keenan et al. (1986) and the transition probability given by Nussbaumer & Storey (1981). This collision strength differs by $\approx$10% from the collision strength calculated by Hayes & Nussbaumer (1984) but is more than 35% larger than the collision stength in Spitzer (1978). We have neglected all radiative processes except spontaneous decay, and we have also neglected cascades and photon pumping. In cold neutral gas, all of the processes in equation (5) can be important, but in warm ionized gas and H II regions, electron collisions are the dominant excitation process and spontaneous radiative decay is the dominant de-excitation process, so equation (5) reduces to

$$\frac{n_2}{n_1} = \frac{n_e \gamma_{12}(e)}{A_{21}}. \quad (6)$$

Thus the presence of C II absorption at velocities where C II* is absent can be used to set upper limits on the electron and hydrogen densities. For example, for HD 168941 at $v = -75$ km s^{-1}, $\tau(\text{C II}) \geq 3$ while $\tau(\text{C II*}) \leq 0.07$. If the absorption originates in warm ionized gas with $T_e \approx 6000$ K, then $\gamma_{12}(e) = 1.52 \times 10^{-7}$ cm^3 s^{-1} and $n_e \leq 0.4$ cm^{-3}.

Cowie & York (1978) and Cowie et al. (1979) have suggested that the correlation of velocity structures (especially velocity extremes) between neutral, low, and high ionization stages indicates that the highly ionized gas resides in interfaces between the ambient hot ISM and cooler clouds. We note in

passing that many, but not all, of the velocity extremes in the four sight lines presented in this paper qualitatively appear to be correlated.

8. SUMMARY

We have observed HD 167402, HD 168941, HD 172140, and HD 173502 with the *International Ultraviolet Explorer* in the high dispersion mode. These stars are distant ($d > 6$ kpc), and the large column densities accumulated on the long paths improve the *IUE*'s ability to detect absorption by highly ionized gas. These stars are also at low Galactic longitudes ($2\overset{\circ}{.}3 < l < 5\overset{\circ}{.}8$), and consequently evidence of radial inflow or outflow is more easily distinguished from Galactic rotation. The principal results are the following:

1. The individual spectra have signal-to-noise ratios of approximately 5 to 10. We obtained new observations of HD 167402 and HD 168941 with the stars offset along the long axis of the *IUE* entrance aperture in order to smear out the fixed pattern noise. Co-adding these offset spectra with aperture-centered observations results in signal-to-noise ratios of approximately 15 to 25.

2. As part of our interstellar study, we have reviewed the stellar classifications. On the basis of UV stellar photospheric and wind lines, we classify HD 167402, HD 168941, HD 172140, and HD 173502 as B0 II/B0.5 Ib, O9.5–9.7 II–III, B0.5 III, and B0.5 III, respectively. These classifications imply that the stars are situated at line-of-sight distances ranging from 6.1 to 6.8 kpc $\pm$ 25% and are 0.69 to 1.5 kpc below the plane.

3. Low and high ion interstellar absorption profiles (including high resolution and S/N optical Ca II profiles) observed toward three of the four stars show significant amounts of absorption extending to -100 km s^{-1}. Negative velocities are not allowed by normal Galactic rotation in the directions sampled. For absorption by gas with a modest radial velocity dispersion (30 km s^{-1}) blurred by the *IUE* instrumental resolution we would expect to detect absorption extending to ~ -40 km s^{-1}.

4. The most plausible interpretation of the forbidden velocity absorption is that we are seeing absorption by outflowing gas at moderate distances from the Galactic plane ($z \approx -560$ to -1080 pc) associated with the 3 kpc arm. This negative velocity gas is consistent with the recent numerical studies by Martos & Cox (1993) of gas flows in the vicinity of spiral arms.

5. Interstellar absorption by N V, C IV, and Si IV is seen toward each star. The high quality composite spectra of HD 167402 and HD 168941 are suitable for determining $N_a(v)$, apparent column density per unit velocity, for each of these species.

6. The high ion column densities and ion ratios toward HD 167402 and HD 168941 appear representative of those previously observed toward inner Galaxy stars. The presence of N V implies the existence of hot ($T \approx 2 \times 10^5$ K) gas along all distant inner Galaxy sight lines so far studied.

7. Interstellar absorption by both Si IV and N V is difficult to understand with those classes of halo gas models only involving photoionization in warm gas or only involving collisional ionization in hot gas. Composite models incorporating photoionization to produce the Si IV and collisional ionization to produce the N V may be required. The self-ionizing radiation emitted by a cooling hot plasma may be an important source of energetic photons.

We thank U. J. Sofia for assistance with the *IUE* observations. We also thank the *IUE* observatory staff for their help in acquiring and processing the data. T. M. T. thanks Marco Martos and Linda Sparke for helpful discussions. This work was carried out using the computing facilities of the Midwest Astronomical Data Reduction and Analysis Facility and also benefitted from the use of MSEARCH at the Colorado *IUE* RDAF for retrieval of *IUE* archival data. This research was supported through NASA grant NAG5-1806, and T. M. T. is supported by the NASA Graduate Student Researchers Program through grant NGT51003.

REFERENCES

Albert, C. E. 1983, ApJ, 272, 509
Bania, T. M. 1980, ApJ, 242, 95
Barker, A. K. 1984, AJ, 89, 899
Begelman, M. C., & Fabian, A. C. 1990, MNRAS, 244, 26P
Berkhuijsen, E. M., Haslam, C. G. T., & Salter, C. J. 1971, A&A, 14, 252
Bianchi, L., & Bohlin, R. C. 1984, A&A, 134, 31
Binney, J., Gerhard, O. E., Stark, A. A., Bally, J., & Uchida, K. I. 1991, MNRAS, 252, 210
Black, J. H., Dupree, A. K., Hartmann, L. W., & Raymond, J. C. 1980, ApJ, 239, 502
Blitz, L., & Spergel, D. N. 1991, ApJ, 379, 631
Bregman, J. N. 1980a, ApJ, 236, 577
———. 1980b, ApJ, 237, 280
Bregman, J. N., & Harrington, P. J. 1986, ApJ, 309, 833
Burks, G. S., York, D. G., Blades, J. C., Bohlin, R. C., & Wamsteker, W. 1991, ApJ, 381, 55
Burton, W. B. 1985, A&AS, 62, 365
———. 1992, The Galactic Interstellar Medium, Saas-Fee Advanced Course 21 (Berlin: Springer)
Clemens, D. P. 1985, ApJ, 295, 422
Cohen, R. J. 1975, MNRAS, 171, 659
Cohen, R. J., & Davies, R. D. 1976, MNRAS, 175, 1
Courtes, G. 1972, Vistas Astron., 14, 81
Cowie, L. L., Jenkins, E. B., Songaila, A., & York, D. G. 1979, ApJ, 232, 467
Cowie, L. L., Taylor, W., & York, D. G. 1981, ApJ, 248, 548
Cowie, L. L., & York, D. G. 1978, ApJ, 220, 129
Cox, D. P. 1991, in IAU Symp. 144, The Interstellar Disk-Halo Connection in Galaxies, ed. H. Bloemen (Dordrecht: Kluwer), 143
Danly, L., Lockman, F. J., Meade, M. R., & Savage, B. D. 1992, ApJS, 81, 125
de Kool, M., & de Jong, T. 1985, A&A, 149, 151
de Vaucouleurs, G. 1964, in IAU Symp. 20, The Galaxy and the Magellanic Clouds, ed. F. J. Kerr & A. W. Rodgers (Sydney: Australian Academy of Science), 195
Diplas, A., & Savage, B. D. 1993, in preparation
Edgar, R. J., & Chevalier, R. A. 1986, ApJ, 310, L27
Fransson, C., & Chevalier, R. A. 1985, ApJ, 296, 35
Garrison, R. F., Hiltner, W. A., & Schild, R. E. 1977, ApJS, 35, 111
Harris, A. W., & Sonneborn, G. 1987, in Exploring the Universe with the *IUE* Satellite, ed. Y. Kondo (Dordrecht: Reidel), 729
Hartquist, T. W., Pettini, M., & Tallant, A. 1984, ApJ, 276, 519
Hayes, M. A., & Nussbaumer, H. 1984, A&A, 134, 193
Heck, A. 1987, in Exploring the Universe with the *IUE* Satellite, ed. Y. Kondo, (Dordrecht: Reidel), 121
Heiles, C. 1984, ApJS, 55, 585
Hill, P. W. 1970, MNRAS, 150, 23
Houck, J., & Bregman, J. N. 1990, ApJ, 352, 506
Iwan, D. 1980, ApJ, 239, 316
Johnson, H. L. 1963, in Basic Astronomical Data, ed. K. A. Strand (Chicago: Univ. Chicago Press), 214
Joseph, C. L., & Jenkins, E. B. 1991, ApJ, 368, 201
Keenan, F. P., Lennon, D. J., Johnson, C. T., & Kingston, A. E. 1986, MNRAS, 220, 571
Koo, B.-C., Heiles, C., & Reach, W. T. 1992, ApJ, 390, 108
Lamers, H. J. G. L. M., Gathier, R., & Snow, T. P. 1982, ApJ, 258, 186
Lindblad, P. O. 1974, in Highlights of Astronomy, ed. G. Contopoulos (Dordrecht: Reidel), 381
Lockman, F. J. 1984, ApJ, 283, 90
———. 1991, in IAU Symp. 144, The Interstellar Disk-Halo Connection in Galaxies, ed. H. Bloemen (Dordrecht: Kluwer), 15
Martos, M., & Cox, D. P. 1993, in preparation
Massa, D. 1989, A&A, 224, 131
Mihalas, D., & Binney, J. 1981, Galactic Astronomy, 2d ed. (San Francisco: Freeman)
Moore, D. W., & Spiegel, E. A. 1968, ApJ, 154, 863
Morton, D. C. 1976, ApJ, 203, 386
———. 1991, ApJS, 77, 119

Nussbaumer, H., & Storey, P. J. 1981, A&A, 96, 91
Oort, J. H. 1977, ARA&A, 15, 295
Pettini, M., & West, K. A. 1982, ApJ, 260, 561
Prinja, R. K. 1988, MNRAS, 231, 21P
Prinja, R. K., et al. 1992, ApJ, 390, 266
Prinja, R. K., Barlow, M. J., & Howarth, I. D. 1990, ApJ, 361, 607
Prinja, R. K., & Howarth, I. D. 1986, ApJS, 61, 357
———. 1988, MNRAS, 233, 123
Prinja, R. K., Howarth, I. D., & Henrichs, H. F. 1987, ApJ, 317, 389
Sanders, R. H., Wrixon, G. T., & Penzias, A. A. 1972, A&A, 16, 322
Saraber, M. J. M., & Shane, W. W. 1974, A&A, 36, 365
Savage, B. D., Cardelli, J. A., Bruhweiler, F. C., Smith, A. M., Ebbets, D. C., & Sembach, K. R. 1991, ApJ, L57
Savage, B. D., Jenkins, E. B., Joseph, C. L., & de Boer, K. S. 1989, ApJ, 345, 395
Savage, B. D., Lu, L., Weymann, R. J., Morris, S. L., & Gilliland, R. L. 1993a, ApJ, 404, 124
Savage, B. D., & Massa, D. 1987, ApJ, 314, 380
Savage, B. D., Massa, D., & Sembach, K. 1990, ApJ, 355, 114 (Paper I)
Savage, B. D., & Sembach, K. R. 1991, ApJ, 379, 245
Savage, B. D., Sembach, K. R., & Cardelli, J. A. 1993b, ApJ, submitted
Sembach, K. R., Danks, A., & Savage, B. D. 1993, A&AS, in press
Sembach, K. R., Savage, B. D., & Massa, D. 1991, ApJ, 372, 81 (Paper II)
Sembach, K. R., & Savage, B. D. 1992, ApJS, 83, 147 (Paper III)
Shapiro, P. R. 1991, in IAU Symp. 144, The Interstellar Disk-Halo Connection in Galaxies, ed. H. Bloemen (Dordrecht: Kluwer), 417
Shapiro, P. R., & Benjamin, R. A. 1991, PASP, 103, 923
Shapiro, P. R., & Moore, R. T. 1976, ApJ, 207, 460
Slavin, J. D., Shull, J. M., & Begelman, M. C. 1993, ApJ, 407, 83
Snow, T. P. 1977, ApJ, 217, 760
Spitzer, L. 1978, Physical Processes in the Interstellar Medium (New York: Wiley)
Tomisaka, K. 1991, in IAU Symp. 144, The Interstellar Disk-Halo Connection in Galaxies, ed. H. Bloemen (Dordrecht: Kluwer), 407
van der Kruit, P. C. 1970, A&A, 4, 462
Wakker, B. P. 1991, in IAU Symp. 144, The Interstellar Disk-Halo Connection in Galaxies, ed. H. Bloemen (Dordrecht: Kluwer), 27
Wakker, B. P., & van Woerden, H. 1991, A&A, 250, 509
Walborn, N. R. 1972, AJ, 77, 312
———. 1973, AJ, 78, 1067
———. 1982, AJ, 87, 1300
Walborn, N. R., Nichols-Bohlin, J., & Panek, R. J. 1985, *International Ultraviolet Explorer* Atlas of O-Type Spectra from 1200–1900 Å (NASA Ref. Pub. 1155)
Walborn, N. R., & Panek, R. J. 1984, ApJ, 280, L27
Weaver, H. 1974, in Highlights of Astronomy, ed. G. Contopoulos (Dordrecht: D. Reidel), 423
Weinberg, M. D. 1992, ApJ, 384, 81